

Climate Change and Economic Growth: An Empirical Study of Economic Impacts of Climate Change

Menghan Yuan

NORD UNIVERSITY BUSINESS SCHOOL

**Climate Change and Economic Growth:
An Empirical Study of Economic Impacts
of Climate Change**

Menghan Yuan

PhD in Business
Nord University Business School

PhD in Business no. 87 (2021)

Climate Change and Economic Growth: An Empirical Study of Economic Impacts of Climate Change

Menghan Yuan

© Menghan Yuan, 2021

ISBN: 978-82-92893-77-7

ISSN: 2464-4331

Print: Trykkeriet NORD

Nord University

N-8049 Bodø

Tel: +47 75 51 72 00

www.nord.no

All rights reserved.

No part of this book may be reproduced, stored in a retrieval system, or transmitted by any means, electronic, mechanical, photocopying or otherwise, without the prior written permission from Nord University

Acknowledgements

Standing before the finishing line and reflecting on the journey through out my PhD, I am grateful to so many wonderful people that have been extremely helpful and supportive to my PhD study. Undertaking the PhD has been a life-changing experience for me and it would not have been possible to do without the tremendous understanding and encouragement I received from many people in the past few years.

First and foremost, I would like to express my sincerest gratitude to my main supervisor, Thomas Leirvik. He always provides all assistance without reservation and he guides me to see how I could strive for the best of my future. I am deeply grateful for your encouraging supervision as PhD study has been challenging and even at the moments of stagnation and frustration, he never stops being positive and inspiring for me.

Many thanks also to Trude Storelvmo and Martin Wild who have been providing invaluable research insights from their expertise of climate science. Given that I am working on an interdisciplinary field of climate and economy, it is of critical importance to have contribution from researchers of various backgrounds. They provided extremely practical contributions to my research.

I greatly appreciate the support received from my co-supervisor Prof. Peter C.B. Phillips, who is really influential in shaping my empirical research methods and critiquing my results. I also thank him for inviting me to visit Yale University, as well as Prof Tony Smith who hosted me during the research stay. The experience provided me precious opportunities to enhance my research competence through Econometrics training and to develop research ideas that were conducted later during the course of PhD.

I am also very grateful to all those at Nord University Business School, especially Ellen Abelgård and Grete Knudsen. Not only has Ellen been so helpful with resolving all kinds of difficulties at work, she is also an attentive friend who makes efforts in helping me to better integrate into the local community and making me feel welcome in Norway. Special thanks to Grete for your a great amount of assistance throughout my research project.

My deep appreciation goes out to the local PhD students and faculty: Pamela Ogada, Yevheniia Antoniuk, Samuel Sarkodie, Kseniya Pak, Valeria Nyu, Vu Le Tran, Anastasiya Henk, Silje Aakre, and Beate Vading. Many thanks for their dedication in discussing research ideas with me and their friendship and warmth they extended to me.

And finally I would like to say a heartfelt thank you to my parents for always believing in me and encouraging me to follow my dreams. And to my dearest friend, Linqi Wang, for convincing me to pursue a doctoral degree. Without her, I could not have embarked this marvelous journey in the first place. And many thanks to Linqi Wang, Haomin Wang, and Xiaodi Guo for being such reliable allies whenever I need them, making it possible for me to finish what I started.

Bodø, May 2021

Menghan Yuan

Abstract

Researchers have made significant advancements in answering whether and how climatic conditions influence societies and the performance of economies for decades. However, large uncertainties exist that prevent us from providing consistent climate projections for a given future emission scenario, which has obvious consequences for society's ability to take necessary mitigation and adaptation action. Climate sensitivity, which measures how much global temperature will change after a doubling of greenhouse gases compared to preindustrial times, has been widely used in climate-economic models that translate climate change into economic damages, and therefore is of highly concern to policy makers to inform climate policies. The goal of this thesis is to constrain the uncertainty of climate sensitivity and to investigate the economic impacts of climate change.

This thesis consists of four papers. The first two papers aim to address the uncertainty of climate sensitivity. In our empirical estimation framework, we relate temperature to solar radiation and CO_2 in a cointegrating equilibrium relationship. However, there is no readily available solar radiation dataset that currently provides observations with global coverage. The first paper resolves the dataset problem by implementing a spatial interpolation method to an observation-based solar radiation dataset. Using a wide range of explanatory variables, we apply a machine learning method, Random Forest, to predict solar radiation at unsampled locations. The output from this paper is a global dataset with complete global land surface coverage during the period 1961-2019, which provides the input data for the climate sensitivity estimation conducted in the second paper.

The second paper empirically estimates Transient Climate Sensitivity (TCS) for 22 global climate models and significantly narrows the confidence interval of TCS compared to previous estimates. Using the constrained distribution of TCS, we further examine its implications to the social cost of carbon. In alignment with the warming target of 1.5°C under the Paris agreement goals, the revised TCS leads to a remaining carbon budget of around nine years of current CO_2 emissions. Compared to the unconstrained reported TCS values in the Coupled Model Intercomparison Project (CMIP6), our narrowed TCR confidence interval suggests a median reduction in the remaining carbon budget of approximately one year of allowable CO_2 emission.

The third and fourth paper use panel data analyses to examine how agriculture and aggregated economies are influenced by climate change. The third paper investigates regional heterogeneity in the effects of climate change on soybean yields. We find statistically significant difference in yield sensitivities to climate change among various regions. A global homogeneous model suggests predominantly negative effects of a warmer climate; however, a regional model of Southeast Asia indicates that local soybean yields could be enhanced in countries located on the northern, cooler fringes of this region. Moreover, we find soybean yields in developed countries, such as the US, Canada, Australia, and European countries, tend not to be significantly affected by climate change.

Following the empirical framework from the third paper, the fourth paper further examines realized impacts of historical climate change on aggregate economic outputs. We find that European and Central Asian countries have benefited both from temperature rising and precipitation fluctuations; on the other hand, a double whammy has been observed in Africa, the trends toward a warmer and dryer climate have both impeded local economic growth.

Contents

Acknowledgements	i
Abstract	iii
Contents	v
1 Introduction	1
1.1 Theoretical Background	1
1.2 Fundamental Approaches and Data Availability	7
1.2.1 Spatial Interpolation	8
1.2.2 Trend Analysis	12
1.2.3 Panel Data Analysis	14
1.2.4 Data Availability	17
1.3 Philosophy of Science	18
1.4 Overview of Four Papers	20
1.4.1 Paper 1: Global Trends in Downward Surface Solar Radiation from Spatial Interpolated Ground Observations during 1961-2019	21
1.4.2 Paper 2: High-sensitivity Earth System Models most Consistent with Observations	22
1.4.3 Paper 3: Heterogeneity in Climate Change Effects on Soybean Yields	22
1.4.4 Paper 4: The Relative Role of Temperature and Precipi- tation in Global Economic Growth	23

2	Global Trends in Downward Surface Solar Radiation	29
2.1	Introduction	30
2.2	Datasets and Method	33
2.2.1	Method	33
2.2.2	Datasets	35
2.3	Results	36
2.3.1	Estimation and Evaluation	36
2.3.2	Interpolated SSR Dataset Trend Analysis	39
2.4	Discussion	58
3	High-sensitivity Earth System Models most Consistent with Observations	67
4	Heterogeneity in Climate Change Effects on Soybean Yields	83
4.1	Introduction	84
4.2	Data and Method	87
4.2.1	Data	87
4.2.2	Empirical Framework	88
4.3	Results	90
4.3.1	Descriptive Statistics	90
4.3.2	Panel Results	95
4.4	Discussion	100
5	Relative Role of Temperature and Precipitation in Economic Growth	107
5.1	Introduction	108
5.2	Data and Method	110
5.2.1	Data	110
5.2.2	Econometric Model	110
5.3	Empirical Results	112
5.3.1	Dataset description	112
5.3.2	Empirical Estimation	113
5.4	Discussion	121

Appendices	127
A Supporting Information for Paper 1	129
A.1 Dataset Description	129
A.2 RF model Parameter Tuning	129
A.3 Results	129
A.3.1 Model Evaluation	129
A.3.2 Continental Average Trend Analysis	130
B Supporting Information for Paper 2	139
B.1 Econometric Framework	139
B.1.1 Model Description	139
B.1.2 Estimation Method	141
B.1.3 Conversion from Global TCR to Land TCR	142
B.2 Data Availability	143
B.2.1 Climate Observations	143
B.2.2 Climate Simulations	144
B.2.3 CO_2 equivalent emissions	145
B.2.4 Reported TCR	145
B.3 Empirical Results	145
B.3.1 Land-Ocean Warming Ratio	145
B.3.2 TCR estimates	147

CHAPTER 1

Introduction

1.1 Theoretical Background

Climate Trends

A growing body of evidence indicates that Earth's climate is changing in general, and the temperature in particular. Weather patterns are changing, disrupting national economies and affecting lives. The global surface temperature has been progressively increased. During the past century (1900-2000), the global average temperature has increased by 0.74°C ; moreover, more than a half of the warming was observed in the last two decades of the period (a rise of 0.38°C happened in 1980-2000) (Scafetta and West, 2005). According to Duan et al. (2021), the warming rate in the second half of the 20th century is approximately twice as large as in the whole century. The Fifth Assessment Report (IPCC AR5) reported that 2010-2019 was the warmest decade ever recorded and the period of 1983-2012 was the warmest 30-year span over the last 800 years for the Northern Hemisphere.

Hydrological responses to global warming are complicated and vary spatially. It has been reported that global precipitation over land has increased by $\sim 3\%$ over the last century (Gerten et al., 2008), which could indicate less drought on a global scale. However, regional precipitation trends vary considerably—dry areas tend to get dryer and wet areas tend to get wetter. This in fact indicates that areas that experienced droughts in the past, will most likely experience them more often in the future, and areas that rarely experienced droughts in the past will be increasingly less likely to experience droughts in the future. Drying trends are observed over most of Africa, southeast Asia, eastern Australia

and southern Europe, and increased precipitation was found over the central US, Argentina and northern high-latitude areas during 1950-2010 (Dai, 2013). Summer drying has been reported in many parts of the northern subtropics and midlatitudes (Burke and Brown, 2008). Moreover, additional areas of land surface are predicted to be in drought by the end of the century (Burke et al., 2006). Rind et al. (1990) and Jones et al. (1996) projected that, severe drought conditions will increase dramatically, especially at low to midlatitudes, by the middle of the twenty-first century.

Solar radiation is a fundamental determinant of the Global Energy Balance, and a crucial driving force for temperature change and hydrological cycle variation (Budyko, 1969; Obryk et al., 2018). Solar radiation has been a key input for many climate studies that investigate climate sensitivity, its effect on agriculture and other economic sectors. Storelvmø et al. (2016) decomposed observed temperature development into components attributable to changes in greenhouse gas concentrations (CO_2) and surface radiation. The increase in greenhouse gas pulls the temperature up, while the reduction of downward solar radiation drags the temperature down. What we observe is the net effect—the temperature. Phillips et al. (2020) estimated transient climate sensitivity, which is the change in global mean surface temperature for a doubling of CO_2 , using an econometric model that applies surface radiation as one of the inputs. Solar radiation is also of high importance for agricultural management that will need to control the amount of solar radiation in order to stimulate crop growth as well as other applications that deploy solar power energy (Lewis, 2016).

Despite of the importance of solar radiation, there are few available global datasets that provide reliable and representative data describing its evolution. Taking an unbalanced panel dataset of solar radiation, the first paper in this thesis constructs a global solar radiation dataset using a machine learning method, and based on which, global solar radiation trends are summarized. Using the constructed solar radiation dataset, the second paper estimates climate sensitivity, defined as the global average temperature change due to a doubling of atmospheric CO_2 . Our empirical framework relates temperature to solar radiation and CO_2 in a cointegrating equilibrium relationship. Therefore the

constructed dataset in the first paper provides the prerequisite input for the second paper.

Climate change has wide-ranging impacts on the world's economies, including human health, energy use, global food security, etc. I will review here some of the major findings of the social and economic impacts of climate.

Economic Impacts: Agricultural Yields

Agriculture is one of the most directly exposed sectors to the impacts of climate change. Variations in climate processes such as temperature, precipitation, and solar radiation directly affect crop growth and production significantly through photosynthesis, transpiration, respiration, and so on. In particular, variabilities in temperature and precipitation can explain a quarter of the crop yield's variability in non-irrigated plants (Kukal and Irmak, 2018). The importance of temperature, often dominating rainfall, in the production of staple crops (Schlenker et al., 2005; Lobell and Burke, 2008). Crops are sensitive to temperatures during specific stages of the growing cycle. The relationship between crop yields and growing season temperature and precipitation changes is extensively studied. Some regional studies indicate that yield responses differ largely from regions to regions, both in magnitude and signs of the impacts. For example, Indian rice yields have been reduced by 5.7% during 1966-2002 under historical trends in temperature, monsoon characteristics, and rainfall (Auffhammer et al., 2012). In the case of Sub-Saharan Africa, substantial losses for aggregate production are predicted—a reduction of -22 and -17% are estimated for maize and sorghum by 2050, respectively (Schlenker and Lobell, 2010). On the other hand, Kucharik and Serbin (2008) found that a trend towards warmer and drier conditions could support higher corn and soybean yields in northern Corn Belt locations that have a cooler climate in general.

In spite of the reported regional difference in crop yields responses to climate change, few studies have explicitly considered parameter heterogeneity in empirical models. Current studies primarily assume homogeneous sensitivities for all regions, and the difference in realized responses is because of the different initial temperatures for various regions (see e.g., Dell et al., 2012; Burke et al., 2015; Diffenbaugh and Burke, 2019). In the third paper of this

thesis, by including regional dummies in our global empirical framework, we explicitly explore the regional heterogeneity in crop yield responses to changes in temperature and precipitation, and thereby obtain region-specific response functions for six regions comprising the world.

Economic Impacts: Aggregate Production

Rather than focusing on individual or sectoral responses to climate, an alternative “top-down” approach examines how the macro-economy as a whole responds to climate change. Studies in this category use gross domestic product per capita (GDPPC) as the variable of interest. Recent studies have shown that temperatures have a nonlinear effect on economic production, such that output is maximized at 13°C (see [Figure 1.1](#), [Burke et al., 2015](#)). In other words, the parabolic relationship between temperature and economic growth indicates that countries with an annual average above 13°C will see a reduction in GDPPC with increased warming, whereas countries with an annual average below 13°C , such as Brazil and India, will experience an increase in economic production. For countries with an annual average below the optimum, for example, Germany and France, the economic output will increase until the optimum is reached.

There is of course a lot of heterogeneity between countries that have a hot annual average temperature, but many of those countries are located in Africa, close to the equator. These countries are already hot and poor, and many of them have a poorly developed infrastructure to mitigate even harsher climatic conditions. Australia, on the other hand, has also above the global optimum temperature, but with a very high GDPPC, highly developed infrastructure, and yet experiences a warming trend in temperature ([Bureau of Meteorology, 2020](#)). The implication is that there is plenty of heterogeneity in how countries with an annual average temperature above the global optimum are able to handle a further increase in temperature. Moreover, [Diffenbaugh and Burke \(2019\)](#) found that global warming has increased global economic inequality. Given that hot countries tend to be poor, with national income falling 8.5% per degree $^{\circ}\text{C}$ in the world cross section ([Dell et al., 2009](#)), it is very likely that poor countries are worse-off while rich countries are better-off under continued global warming. In particular, [Diffenbaugh and Burke \(2019\)](#) indicated that the ratio of GDP

per capita between the top and bottom decile countries are 25% larger than in a world without global warming.

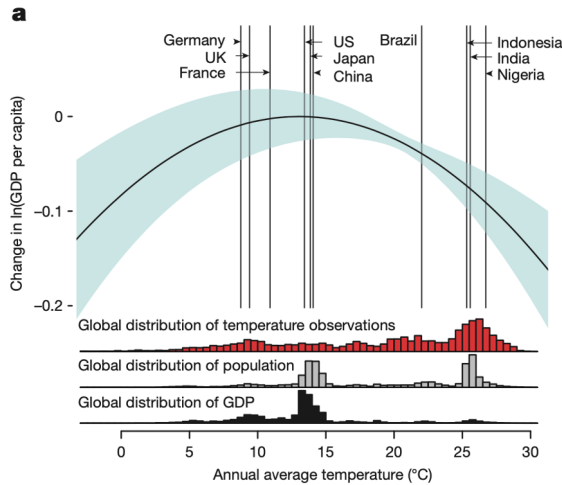


Fig. 1.1 Effects of annual average temperature on economic production. The figure is taken from [Burke et al. \(2015\)](#). Vertical lines indicate average temperature for selected countries. Histograms show global distribution of temperature exposure (red), population (grey), and income (black).

The scientific interest in the effects of rainfall on economic growth has grown significantly, however, only a limited number of studies deliver conclusive results. [Berlemann and Wenzel \(2018\)](#) found statistically significant negative impacts of rainfall shortages on economic growth, but the effects are only specific to developing countries where economies are largely dependent on rainfed agriculture. This indicates that the effects of precipitation on an economy are mainly realized through agriculture. [Berlemann and Wenzel \(2018\)](#) also reported that rainfall surpluses have no significant growth effects. [Schlenker and Lobell \(2010\)](#) further corroborated the effects of low precipitation by indicating that low precipitation has slowed GDP growth in Africa.

In the fourth paper, we examine realized impacts of observed temperature and precipitation evolution for countries worldwide. Our results show dominant effects of temperature as compared to precipitation, moreover, regions have responded considerably differently. Specifically, Europe and Central Asia have benefited from both historical temperature and precipitation trends, whereas

a double whammy has been observed in Africa, resulting in economic growth being slowed down by both factors.

Health Impacts

Climate change is also found to have severe implications for human health, and even though I do not directly address this in my thesis, health and economic productivity is closely related (see e.g., [Ivinson, 2002](#); [Bhargava et al., 2001](#)). Good health has a positive and statistically significant effect on aggregate output ([Bloom et al., 2004](#)). Healthier workers are physically and mentally more energetic and productive at work places, thereby boosting economic growth and development.

As individuals, each of us is constantly exposed to temperature, and our health could be compromised under extreme heat or cold, which could lead to severe cardiovascular, respirator, and cerebrovascular effects that can result in death ([Deschenes, 2014a,b](#); [Carleton and Hsiang, 2016](#)). For example, in Delhi, deaths increase by 3.2% per $^{\circ}C$ above $20^{\circ}C$, and in the US, days above $32.2^{\circ}C$ and below $-6.7^{\circ}C$ increases male mortality rate by 2% and 1.4%, respectively ([Barreca et al., 2016](#)). In addition to these mortality damages, many injuries from temperature extremes are not lethal. During high and low daily temperatures, hospital admissions increase for respiratory and cardiovascular diseases. In particular, besides temperature, humidity was found to be an critical determinant of human influenza, which is a notable cause of hospitalization in temperate climates ([Barreca and Shimshack, 2012](#)).

Transmission and distribution of vector-borne disease are greatly influenced by environmental and climatic factors (see e.g., [Gething et al., 2011](#); [Craig et al., 1999](#)). Accordingly, it has been suggested that the dynamics and distribution of a range of vector-borne diseases, including malaria, dengue fever, viral encephalitis, schistosomiasis, Lyme disease, could be impacted by climate change (see e.g., [Paaijmans et al., 2012](#)). Temperature regimes constrain the geographical extent of the disease and contribute to determining its intensity. Generally, transmission intensity is assumed to be higher under warmer conditions, where parasites and pathogens within vectors increase fast. For example, transmission intensity of malaria are largely influenced by mosquito and parasite life history traits

(e.g., adult mosquito longevity, biting rate), which are strongly temperature sensitive (Carballar-Lejarazú et al., 2020; Scudellari, 2019). Shapiro et al. (2017) suggested a temperature optimum for transmission of 29°C , with minimum and maximum temperatures of 12 and 38°C , respectively. Anthropogenic climate change is likely to shift disease ranges and increase exposure globally, more research is need to quantify the link between changing temperatures, rainfall, and public health (Bhatt et al., 2013; Gething et al., 2010).

Temperature extremes also impact performance of workers, especially for factory or labor intensive manual work. Optimal temperature for worker performance is between 21 to 25°C , while beyond that range, too hot or too cold temperatures are harmful for productivity (Seppanen et al., 2003). When the temperature is above 25°C , Seppanen et al. indicated an average 2% decrement in work performance with an temperature increase of 1°C .

1.2 Fundamental Approaches and Data Availability

In this section, I will present some fundamental tools for economic analyses of climate change. These models constitute the prototypes of models applied in my thesis. I will first talk about *Spatial interpolation*, which is applied in the first paper to tackle the missing data problem in climatic datasets. Measuring climate change is an essential component of climate economic studies and is constantly discussed through out the thesis; therefore, I will then talk about *trend analysis* techniques frequently applied in climate science.

Panel data analysis is one of the most frequently used approaches in empirical studies of climate change. Paper 2 to 4 all applied panel approaches either to obtain estimates of critical parameters in climate models or to make inference of economic damages from climate change. Therefore, some elementary issues of panel data analysis are discussed briefly.

At last, I will introduce data availability related in the thesis, including weather datasets, climate model directories, and databases of economic indicators.

1.2.1 Spatial Interpolation

To study the trends and impacts of climate, it is of the utmost importance to have reliable data, which can be used for analyzing a wide range of global, and local, aspects of the environment. Global air temperature has become the primary metric for measuring global climate change. The overall increase of global temperature over the last century has been largely attributed to the increase of greenhouse gases (Flato and Marotzke, 2013). Besides the effects of greenhouse gases, solar radiation has been a major driver of temperature variability (Wang and Dickinson, 2013). Storelvmo et al. (2016) show that observed temperature trends can be decomposed into components attributable to changes in greenhouse gas concentrations and surface radiation. The effects of solar radiation impacts on temperature are primarily explained through changes in atmospheric aerosol loading, such as SO_2 , which has a cooling effect. In particular, Storelvmo et al. (2016) find that the solar radiation trends have caused a cooling that masked approximately one-third of global warming over the past half-century.

In order to measure global temperature dynamics and climate change, it is essential to have datasets that have complete spatial coverage and have climatic observations for a relative long term. Such datasets are readily available for temperature and CO_2 , however, there are few, if any, complete datasets for solar radiation over a long time period for many locations. One such dataset is the Global Energy Balance Archive (GEBA, Wild et al., 2017). The GEBA dataset has a long time range, with the first observations from the early 1950's, continuing to the present day. However, many values are missing due to maintenance and operational failures of observation devices. Therefore, paper 1 addresses the missing value problem in the GEBA dataset, aiming to construct a solar radiation dataset with complete spatial coverage and containing data for a long period.

To fill missing values, many different techniques have been tested, with linear interpolation as one of the simplest. This, however, does not perform very well if there are several consecutive missing values, and in particular if the data is seasonal, which is certainly true for solar radiation. Other, more advanced, techniques used by researchers are, for example, Inverse Distance Weighting

(IDW), Kriging, splining, regression and etc. (see e.g., Collins, 1995; Scudiero et al., 2016; Erxleben et al., 2002). We applied advanced statistical methods, often called machine learning techniques, to fill any missing values in the solar radiation dataset.

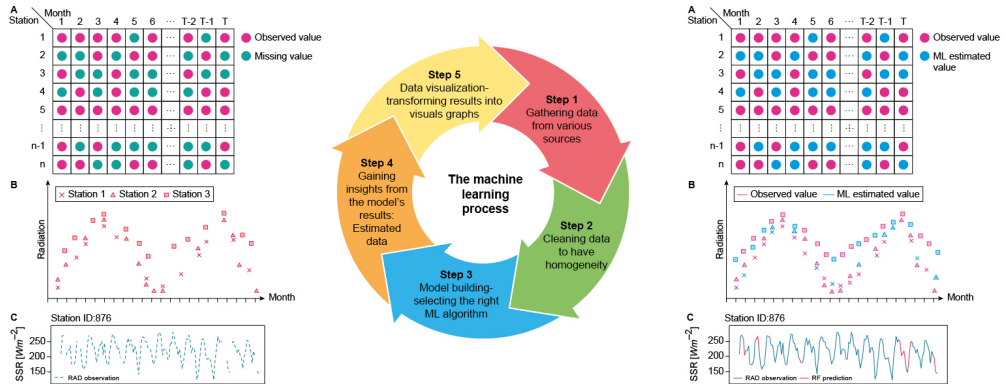


Fig. 1.2 A graphical illustration of the original and the output data, and how the machine learning method is implemented to implement the spatial interpolation. Figure is taken from Leirvik and Yuan (2021).

Figure 1.2 shows a diagram of how we implemented spatial interpolation in paper 1. Panel A in the left column of Figure 1.2 illustrates our initial dataset, where the y-axis is the station and the x-axis is time. Thus, each geographical station measures solar radiation at time t . An observation is illustrated with a red colored circle. However, some observations are missing, and are represented by the green colored circles. Our objective is to apply various quantitative methods to the values illustrated by the green circles. Estimates from machine learning techniques are represented by the blue circles in Panel A, in the right column of Figure 1.2. Panels B in the left and right column illustrate three hypothetical stations with solar radiation values, points in time where the solar radiation is missing (left column), and how the solar radiation time series would be after inserting the estimates of solar radiation (right column) for any missing values. Furthermore, Panel C in the left column takes a randomly selected station with actual observations and missing values, and plots the solar radiation of the time-period analyzed. Panel C in the right column illustrates a complete solar radiation time series with both estimated and observed values of the solar

radiation. The middle column in [Figure 1.2](#) illustrates the machine learning process applied in the paper and how it is used to achieve the results.

Frequently applied spatial interpolation methods are briefly explained at what follows. IDW is a deterministic estimation method where the value at a missing location is determined by weighted average of values at neighboring points, where the weights are assigned as inversely proportional to the distance from the target location. Although its simplicity makes it easy to implement, a drawback is that it will have a discontinuous slope of the estimation surface at each data point ([Collins, 1995](#)). The Kriging method is a method of interpolation where the interpolated values are modeled by a more sophisticated relationship between observed values with target missing values. The relationship is depicted by a variogram function, which calculates the semi-variance differences (spatial autocorrelation) between the neighboring values. The variogram can be exponential, spherical, logarithmic or any other functions. Spline models, a class of functions often called polynomial interpolation models, use mathematical functions to connect the sampled data points in order to produce a continuous elevation and grade surface while minimizing the curvature of the surface. These models are useful when the surface varies smoothly without sharp fluctuations. The models mentioned above are univariate, which means that they apply only information about the variable of interest, i.e., the variable with missing values that is desirable to estimate. Regression methods break the limit of using only the target variable for estimating missing values by characterizing the response's relationship with other potential explanatory variables, such as location (latitude, longitude) of measurement station, and other correlated atmospheric variables. Recently, so-called machine learning methods have been applied in spatial interpolation (see e.g., [Jiang, 2008](#); [Sun et al., 2016](#); [Zhou et al., 2017](#)). Machine learning consists of many different statistical models that computer systems use to effectively perform a specific task without using explicit instructions and strong assumptions, it relies mostly on pattern recognition and inference instead. One such method, the Artificial Neural Network (ANN), was implemented for the estimation of monthly mean solar radiation and showed superiority over polynomial fitting models ([Jiang, 2008](#)). Though with its high accuracy, the ANN method has the limitation of computational complexity and

therefore cannot incorporate a large number of explanatory variables. Another alternative machine learning model, the Random Forest (RF) model, provides a solution for accommodating a high dimension of covariates, and has been applied in several recent studies. For example, [Sun et al. \(2016\)](#) presented a RF model to estimate solar radiation based on three types of input variables: sunshine hours, air temperature, and their derivative types. Surface albedo, emissivity and vegetation indices data were used as predictors by [Zhou et al. \(2017\)](#) in the RF model in order to generate an accurate prediction of solar radiation. Most of the research on spatial interpolation is on a regional scale and/or only considers a relatively short period of time for testing model quality, such as a one-year period. The main contribution of this paper is to propose an effective machine learning method in spatial interpolation of Surface Solar Radiation (solar radiation), that is applicable for the global scale and could make use of information from long term trends.

The first objective is to interpolate the solar radiation dataset in GEBA, therefore obtaining a complete dataset of solar radiation with no missing values. Two papers are constructed in this endeavour. Given a variety of interpolation methods available, my supervisor and I started with a performance evaluation of interpolation approaches, which developed into a published paper in *Earth and Space Science* ([Leirvik and Yuan, 2021](#)). This paper applies Random Forest (RF) and seven other conventional spatial interpolation models (Ordinary Kriging, Linear Regression, several types of Regression Kriging) to the GEBA dataset. Based on the trained models, we calculated error metrics of predicted values against observations and found that the RF model significantly outperforms all other models. In particular, we find that the mean absolute error (MAE) of the RF is reduced by 50+% compared to the average MAE of the conventional interpolation methods. This paper is not included in my PhD thesis because it is not applied directly in my climate-economic research.

Given that [Leirvik and Yuan \(2021\)](#) demonstrated the superiority of the Random Forest model, we then applied the model to unsampled areas or time points with no existing observations. In other words, we generated simulations that extend the original dataset both over space and time. The simulation output is a gridded dataset at 0.5° resolution that covers all land surface except

Antarctica and spans the period from 1961 to 2019. Its spatial completeness and the large time span make the constructed dataset a valuable alternative to existing solar radiation datasets. Based on the new dataset, we further analyzed historical solar radiation trends in a regional and global level. The results from this analysis is important and very useful in many areas regarding the climate-human-economic relationship, the results was condensed into a collaborative paper with Thomas Leirvik and Martin Wild, which is revise-resubmit in *Journal of Climate*. I decide not to include [Leirvik and Yuan \(2021\)](#) in this thesis because I deem it as a trial project for preparing the model selection criteria for selecting a spatial interpolation method that is most appropriate for the dataset construction conducted in the first paper of the thesis. The output dataset of the first paper is further applied in the second paper of the thesis for climate sensitivity estimation.

1.2.2 Trend Analysis

Linear Trend Estimation

Climate data is often a univariate time series, $\{y_t\}_{t=1}^T$, that is a sequence of random variables indexed by t . It is critical to understand the rates of change for climate variables, such as temperature, precipitation, and solar radiation. A commonly reported metric is the decadal trend, which measures the average change per decade. We use decadal trends to quantify the average evolution of climate during a long term, and they can be used to inform, for example, whether global warming is accelerating, decelerating, or no change; if there is a persistent trend in rainfall. Trend analysis is applied throughout the thesis, and the results are explicitly reported in the first two papers.

The various studies analyzing long-term trends of surface solar radiation suggests a widespread decrease in surface solar radiation between the 1950s and 1980s (“global dimming”), with a partial recovery more recently at many locations (“brightening”) (see e.g., [Wild, 2009](#); [Sanchez-Lorenzo et al., 2015](#); [Stjern et al., 2009](#)). Several of these studies discuss the brightening in Europe in more detail. [Norris and Wild \(2007\)](#) determined a Pan European time series based on 75 stations from GEBA, and estimated a linear decline of 3.1 Wm^{-2}

decade⁻¹ for the “dimming” period 1971-1986, but an increase of 1.4 Wm^{-2} decade⁻¹ for the “brightening” period 1987–2002. Chiacchio and Wild (2010) pointed out that the brightening in Europe is particularly pronounced in the spring and summer seasons, while there is no evidence for a brightening in the other seasons. Paper 1 contributes to the existing literature by reporting decadal trends of solar radiation for each $0.5^\circ \times 0.5^\circ$ grid cell on the global land surface to inform the global brightening/dimming process.

Trend analysis is also applied in other papers in the thesis. In particular, the second paper calculates the warming trends of global surface temperature using data from climate model output, which are later used as input parameters for climate sensitivity estimation. The third and fourth paper are focused on examining agricultural and economic impacts of climate change, respectively. Climate trends of temperature and precipitation are summarized on a country scale (crop growing season average trends in the third paper and annual average trends in the fourth paper) and realized impacts of historical trends are reported in the fourth paper.

A linear trend of y_t is the estimate of the slope coefficient of a linear regression of y_t on time. The decadal trend can be obtained by multiplying the slope coefficient by 10. Figure 1.3 shows an example of linear trend estimation.

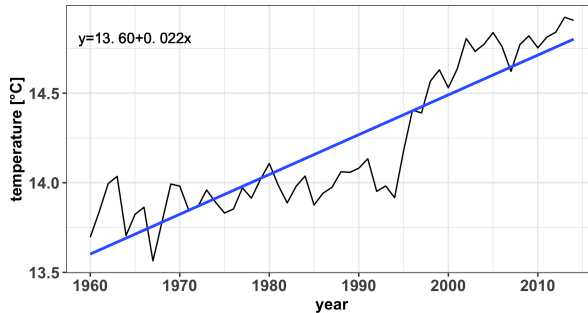


Fig. 1.3 Trend estimation illustration. Black line stands for temperature observations, blue line stands for linear trend approximation. The estimation of the regression equation is shown on the top-left corner of the figure, with the intercept coefficient (β_0) being 13.6 and the linear trend coefficient (β_1) being 0.022. Note that the x-axis (year) is rescaled to start from 0 in the equation estimation.

A linear trend regression model is given by

$$y_t = \beta_0 + \beta_1 T_t + \varepsilon_t \quad (1.1)$$

where $t = 1, \dots, T$, and T_t is the time variable assigned to y_t . β_0 is the intercept and β_1 is the slope coefficient which can be interpreted as the linear trend of y_t .

Eqn. (1.1) can be written in a matrix form

$$\mathbf{y} = \mathbf{X}\boldsymbol{\beta} + \boldsymbol{\varepsilon} \quad (1.2)$$

where \mathbf{y} is a $T \times 1$ vector, and $\boldsymbol{\beta} = (\beta_0, \beta_1)'$, and \mathbf{X} is a $T \times 2$ matrix, with the first column being 1 indicating the intercept constant.

The ordinary least-squares (OLS) estimation minimizes the sum of squared errors (SSE):

$$\text{Minimize}_{\boldsymbol{\beta}} SSE(\boldsymbol{\beta}) = \boldsymbol{\varepsilon}'\boldsymbol{\varepsilon} = (\mathbf{y} - \mathbf{X}\boldsymbol{\beta})'(\mathbf{y} - \mathbf{X}\boldsymbol{\beta})$$

Expanding this gives

$$\boldsymbol{\varepsilon}'\boldsymbol{\varepsilon} = \mathbf{y}'\mathbf{y} - 2\mathbf{y}'\mathbf{X}\boldsymbol{\beta} + \boldsymbol{\beta}'\mathbf{X}'\mathbf{X}\boldsymbol{\beta}$$

The necessary condition for a minimum is

$$\frac{\partial S(\boldsymbol{\beta})}{\partial \boldsymbol{\beta}} = -2\mathbf{X}'\mathbf{y} + 2\mathbf{X}'\mathbf{X}\boldsymbol{\beta} = 0$$

Then the explicit solution is

$$\begin{aligned} \boldsymbol{\beta} &= (\mathbf{X}'\mathbf{X})^{-1}\mathbf{X}'\mathbf{y} \\ &= (\mathbb{E}(\mathbf{X}'\mathbf{X}))^{-1}\mathbb{E}(\mathbf{X}'\mathbf{y}) \end{aligned} \quad (1.3)$$

The OLS moment estimator is therefore given by

$$\begin{aligned} \hat{\boldsymbol{\beta}} &= \left(\frac{1}{T} \sum_{t=1}^T \mathbf{x}_t \mathbf{x}_t' \right)^{-1} \left(\frac{1}{T} \sum_{t=1}^T \mathbf{x}_t y_t \right) \\ &= \left(\sum_{t=1}^T \mathbf{x}_t \mathbf{x}_t' \right)^{-1} \left(\sum_{t=1}^T \mathbf{x}_t y_t \right) \end{aligned} \quad (1.4)$$

1.2.3 Panel Data Analysis

Economists traditionally use the term **Panel data**, also called **longitudinal data**, to refer to data structures consisting of observations on many individuals for multiple time periods. The observed “individuals” can be, for example, people,

households, workers, firms, schools, production plants, industries, regions, states, or countries. The distinguishing feature relative to cross-sectional datasets is the presence of multiple observations for each individual. More broadly, panel data methods can be applied to any context with cluster-type dependence (Hansen, 2019).

Paper 2 uses a panel data structure with stations being individuals, where parameters can be estimated by fully-modified least squares estimators (FM-OLS, refer to paper 3 for details). Paper 3 and 4 apply a panel data structure with countries being individuals. Here I introduce the individual fixed effects model, which consists of the baseline of the empirical frameworks applied in paper 3 and 4. We consider the linear individual effects model given by

$$y_{it} = \mathbf{x}'_{it}\boldsymbol{\beta} + u_i + \varepsilon_i \quad (1.5)$$

or in a matrix form

$$\mathbf{y}_i = \mathbf{X}'_i\boldsymbol{\beta} + \mathbf{1}_i u_i + \boldsymbol{\varepsilon}_i \quad (1.6)$$

where y_{it} is indexed by an individual i and time t , $i = 1, \dots, N$ and $t = 1, \dots, T$, u_i is the individual-specific effect that represents a time-invariant unobserved missing variable. For example, if \mathbf{y}_i represents economic outputs of country i , \mathbf{X}_i represents climate variables, then the individual-specific effects, u_i , will absorb effects of omitted factors that influence the country's historical average economic development, such as history, culture, topography, demography, institutional qualities, etc.

When u_i is interpreted as a missing variable it is natural to expect it to be correlated with the regressors \mathbf{x}_{it} . Correlation between u_i and \mathbf{x}_{it} will cause both pooled and random effect estimators to be biased due to the classic problems of omitted variables bias and endogeneity. If we leave the relationship between u_i and \mathbf{x}_{it} fully unstructured, then the only way to consistently estimate the coefficient $\boldsymbol{\beta}$ is by an estimator which is invariant to u_i . This can be achieved by transformations which eliminate u_i .

On such transformation is the within transformation. I will present here this transformation in detail.

Define the mean of a variable for a given individual as

$$\bar{y}_i = \frac{1}{T_i} \sum_{t \in S_i} y_{it}$$

We call this the individual-specific mean. Subtracting the individual-specific mean from the variable we obtain the deviations

$$\dot{y}_{it} = y_{it} - \bar{y}_i$$

Similarly for the regressors we define the individual-specific means and the demeaned values

$$\bar{\mathbf{x}}_i = \frac{1}{T_i} \sum_{t \in S_i} \mathbf{x}_{it}$$

$$\dot{\mathbf{x}}_{it} = \mathbf{x}_{it} - \bar{\mathbf{x}}_i$$

Taking individual-specific averages to Eqn. (1.6) we obtain

$$\bar{y}_i = \bar{\mathbf{x}}_i' \boldsymbol{\beta} + u_i + \bar{\epsilon}_i$$

where $\bar{\epsilon}_i = \frac{1}{T_i} \sum_{t \in S_i} \epsilon_{it}$. Subtracting from Eqn. (1.6) we obtain

$$\dot{y}_{it} = \dot{\mathbf{x}}_{it}' \boldsymbol{\beta} + \dot{\epsilon}_{it} \tag{1.7}$$

where $\dot{\epsilon}_{it} = \epsilon_{it} - \bar{\epsilon}_i$. By doing so, the individual effect u_i has been eliminated. It can be written in matrix notation

$$\dot{\mathbf{y}}_{it} = \dot{\mathbf{X}}_{it}' \boldsymbol{\beta} + \dot{\boldsymbol{\epsilon}}_{it} \tag{1.8}$$

The OLS estimator to Eqn. (1.8) is

$$\bar{\boldsymbol{\beta}}_{\text{fe}} = \left(\sum_{i=1}^N \sum_{t \in S_i} \dot{\mathbf{x}}_{it} \dot{\mathbf{x}}_{it}' \right)^{-1} \left(\sum_{i=1}^N \sum_{t \in S_i} \dot{\mathbf{x}}_{it} \dot{y}_{it} \right) \tag{1.9}$$

$$= \left(\sum_{i=1}^N \dot{\mathbf{X}}_i' \dot{\mathbf{X}}_i \right)^{-1} \left(\sum_{i=1}^N \dot{\mathbf{X}}_i' \dot{\mathbf{y}}_i \right) \tag{1.10}$$

This is known as the **within** estimator of $\boldsymbol{\beta}$. It is called the within estimator because it is based on the variation of the data within each individual.

1.2.4 Data Availability

Climate Data

Climate scientists have been using climate/weather data to examine long-term trends of climate evaluation and occurrences of extreme weather events (see e.g., [Jones et al., 1996](#); [Burke et al., 2006](#); [Auffhammer et al., 2013](#); [Carleton and Hsiang, 2016](#)). To clarify the difference between climate and weather, climate is a long average of weather at a given location, while weather refers to short term atmospheric conditions. Climate change refers primarily to long-term changes.

There are several main sources of climate data: observations from weather stations, observation-derived products (e.g., satellite data), and climate model simulations. Observations collected from weather stations are regarded as the most reliable, however, they are afflicted with problems about spatial and temporal coverage. This is because it is difficult to main observation stations at mountainous and marine regions; moreover, maintenance and operational failures cause interruptions and discontinuity of observations. Missing value problem is especially typical in solar radiation datasets, because there is no extensive coverage of such observation stations, and existing stations tend to cluster in developed regions, such as Western Europe and North America. However observations for a range of other variables are complete, such as temperature, precipitation, cloud coverage, due to their widespread coverage of weather stations and their well-developed interpolation techniques. Given the disparity in data availability between solar radiation and other climate factors, paper 1 explores the possibility to predict solar radiation using other climate factors as explanatory variables. And it turns out that our selected climate variables can explain more than 90% of the total variation of global solar radiation.

In paper 1, we obtain data of climatic predictors from the Climate Research Unit Time-series data version 4.04 (CRU-TS v.4.04, [Harris et al., 2020](#)). The CRU dataset provides high resolution ($0.5^\circ \times 0.5^\circ$) gridded data of monthly observations for a wide range of meteorological variables over the period 1901-2019. It is derived by the interpolation of monthly climate anomalies from extensive networks of weather station observations. It covers all land domains of the world except Antarctica, and there are no missing values in the defined

domain. CRU dataset is applied in all four papers contained in the thesis. Paper 2 uses the temperature data to estimate climate sensitivity; paper 3 and 4 aggregate gridded temperature and precipitation data to country-level data and, based on which, estimate economic impacts of climate change.

Global Climate Models (GCMs) provide simulations of historical climate and predictions of climate. GCMs are physics-based models based on well-documented physical processes to simulate the transfer of energy and materials through the climate system. They use mathematical equations to characterize how energy and matter interact in different parts of the ocean, atmosphere, land; therefore, they are sometimes also called Atmosphere-Ocean GCMs, Earth System Models (ESMs), or simply, and most commonly, climate models. Paper 2 uses GCM data to estimate climate sensitivity and compares the results with the reported values in order to verify the robustness of our proposed empirical estimation framework. GCM data can be obtained from the Coupled Model Intercomparison Project - Phase 6 archive (CMIP6, [Eyring et al., 2016](#)).

Economic Data

Using country-year panel data, Paper 3 and paper 4 examine the effects of climate change on crop yields and economic growth, respectively. Crop yields data can be obtained from the Food and Agriculture Organization of the United Nations (FAOSTAT, <http://www.fao.org/faostat/en/#data/QC>). Economic indicators are available from the World Bank's World Development Indicators dataset ([WDI, 2020](#)),

1.3 Philosophy of Science

This thesis uses quantitative models to describe natural processes, assess impacts of climate change. The issue of double-counting has long been the subject of debate in the philosophical as well as statistical literature. Double counting is defined as if data have been used to construct a hypothesis, then the data should not be used again as evidence in support of the hypothesis ([Deborah, 2008](#)). That is to say, an accordance between evidence and hypothesis provides a genuine test of hypothesis only if evidence is not used in the hypothesis'

construction. It is believed that double counting has the potential of posing unreliable inferences. For example, if the model is constructed in a certain way that presumes some beliefs, it is highly doubtful an inference that the belief is actually true. Although the inferences were originated from fitting the data, they were constrained to reflect what is real, or at least trying to do so. We shall not reject the existence meaning of hypothesis testing, indiscriminately disparages all procedures that involve double counting will result in negating certain reliable model validation and conclusion, thereby we are not able to generate useful conclusions from data dependent inferences. Therefore, meticulous cautiousness is required when dealing with double counting, it is the condition, property, probativeness of the hypothesis test that determine whether a double use of data in hypothesis testing is acceptable.

[Popper and Notturmo \(1994\)](#) provides a solution for accepting a hypothesis. According to their theory, observations and experiments can be accepted as supporting a theory (or a hypothesis, or a scientific assertion) only if these observations or experiments are severe tests of the theory—or in other words, only if they result from serious attempts to refute the theory, especially from trying to find faults where these might be expected in the light of all our knowledge. Severity here is the probability that the test rejects a hypothesis h when h is false. Requiring severity is similar to requiring a high power of a statistical test to detect the falsity of h . When severity is satisfied we argue that the test is genuinely probative, otherwise a good fit between the data and hypothesis would be very difficult to generate were hypothesis incorrect. When the severity is seriously violated we may conclude that the hypothesis is not determinant in the way that helps to generate a good fit of data, i.e., such a fit could result from a fit even if the hypothesis were false. In conclusion, if the occurrence of a good fit between the data and hypothesis is impossible unless the hypothesis is true, then we could be sure that inference from the hypothesis is correct.

According to [Akaike \(1998\)](#), an unbiased estimate of the predictive accuracy of a model can be obtained by considering both its fit to data and its simplicity, as measured by the number of adjustable parameters it contains. A model should be simple, reduce the redundancy to the maximum degree. In practice,

we give a regulation term to punish the model with more number of parameters. For the complex model to have the higher predictive ability, not only should it fit the data better, but also it fits the data sufficiently better to compensate for the loss in simplicity that it represents (Hitchcock and Sober, 2004).

At last, a caveat that should be kept in mind is that no model is perfect, models can not reflect the reality perfectly, nonetheless we could still at least learn some valuable insights about the world from the models. “All models are wrong, some are useful.” said the famous statistician George Box. We can not pursue perfection in our models, no model can simulate observations with one hundred percentage confidence. There are always randomness in the reality that can not be captured perfectly in the model, probably there are important factors that we neglected, maybe we over simplified reality with unrealistic assumptions. In all, each model is wrong in a different way. Although there is weakness in our model, they are not useless at all. All together they might provide useful perspectives to our problem to solve.

1.4 Overview of Four Papers

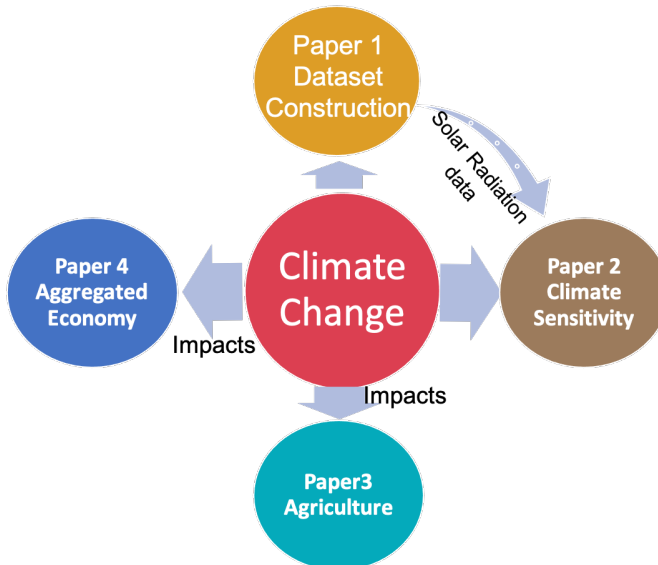


Fig. 1.4 Thesis outline.

Figure 1.4 shows a diagram of the structure of this thesis. The central topic of the thesis is climate change, revolving around which, four papers are developed. In particular, the first two papers altogether constrain the uncertainty of climate sensitivity. The first paper conducts a spatial interpolation to construct a solar radiation dataset that is used in the empirical estimation of climate sensitivity in the second paper. The last two papers are focused on assessing the agricultural and aggregated economic impacts of climate change, respectively. The constructed solar radiation dataset was also applied in the last two papers but the results show that solar radiation is not a significant factor. In what follows, I will provide a summary for each of the four papers consisting of the thesis.

1.4.1 Paper 1: Global Trends in Downward Surface Solar Radiation from Spatial Interpolated Ground Observations during 1961-2019

Paper 1 constructs a high resolution ($0.5^\circ \times 0.5^\circ$) global solar radiation dataset that spans nearly 60 years with monthly frequency and has complete global land surface coverage. The constructed dataset provides the prerequisite input, solar radiation data, for paper 2 that empirically estimates climate sensitivity.

In particular, this paper applies a machine learning method, Random Forest, to interpolate an observational solar radiation dataset. We use a wide range of explanatory variables to predict solar radiation, including climatic variables (e.g., temperature indices, precipitation, cloud coverage, vapour pressure, etc.), time point indicators (year and month), and coordinates of locations (latitude and longitude). The trained Random Forest model has remarkable performance; it is able to capture more than 90% of the total variation of global surface solar radiation. Among the predictors, we find that maximum temperature and month indicator provide the most explanatory power in predicting solar radiation. The trained model is then applied to interpolate solar radiation values for unsampled locations and thereby generating a global dataset with complete land coverage.

Based on the output dataset, we further analyze solar radiation trends on a global and a continental level. We also report seasonal patterns of historical radiation evolution.

1.4.2 Paper 2: High-sensitivity Earth System Models most Consistent with Observations

Paper 2 estimates Earth's Transient Climate Response (TCR), defined as the global mean surface air temperature change due to a doubling of atmospheric CO_2 , at the time of doubling. TCR is a critical parameter for integrated assessment models that are extensively applied by policy makers to evaluate consequences of alternative emission scenarios and inform climate change policy.

Using the solar radiation dataset built from the first paper and other additional climate datasets, we estimated TCRs of 22 global climate models by employing an empirical framework that relates temperature to solar radiation and CO_2 in a cointegrating equilibrium relationship. The empirical TCRs provides a much narrower confidence interval ($2.3 \pm 0.4^\circ C$) as compared to reported TCR by CMIP6 (Coupled Model Intercomparison Project). Using the narrowed distribution of TCR, we calculated the remaining carbon budgets. We find that constrained by a $1.5^\circ C$ warming target that aligned with the Paris agreement goals, we have around nine years of current CO_2 emissions.

1.4.3 Paper 3: Heterogeneity in Climate Change Effects on Soybean Yields

Paper 3 investigates the effects of climate change on soybean yield growth. Based on a panel data analysis approach, we examine how soybean yields response to climate change from both a global and regional level. Under a global homogeneous assumption, we find a non-linear relationship between growing season average temperature and yield growth. In particular, global yield growth minimizes at $24.9^\circ C$, meaning that warming damages are exacerbating until the optimum and, above that, a continual warming is less detrimental probably due to adaption of local crop variety to heat for countries that have been persistently hot. However, our further analyses show evidence that the global response

function is not representative for all individual regions. By including regional dummies to our empirical model, we find significant heterogeneity among regions. For example, for mid- and high-latitude developed countries, temperature is not a significant factor to crop yields growth. Moreover, Southeast Asia shows a strikingly different response curve from the global one. The region indicates a parabola that maximizes at 24.34°C , suggesting northern, cooler countries within the region, such as China, South Korea, and Japan may be beneficiaries of a warmer climate, whereas hot countries situated at the southern fringes will be affected adversely.

Compared to the large regional heterogeneity of temperature responses, the effects of precipitation are more consistent across regions. Despite of the fact that there exist various optimal precipitation levels for various regions, in general, regions will benefit from more precipitation before respective optimums and be harmed by extra precipitation above optimums. We also show the dominant effects of temperature on soybean yields as compared to precipitation.

1.4.4 Paper 4: The Relative Role of Temperature and Precipitation in Global Economic Growth

Paper 4 follows the similar logic of paper 3 but is focused on examining historical impacts of climate change on aggregate economic growth. Based on a panel of 169 countries over the period 1961-2019, we summarized climate changes that have occurred and estimated realized economic impacts of these changes. We find pervasive warming trends for countries worldwide and a majority of them shows a rise of temperature at accelerating rates. We also find that cooler countries exhibit larger magnitude of a rise of temperature as well as larger variability than warmer countries. On the other hand, precipitation shows no evident long-term trends and precipitation varies largely across the years for countries with a large amount of rainfall.

In addition to the conventional country-year fixed effects model (FE), we applied an innovative approach—interactive fixed effects model (IE), which allows heterogeneity to enter the model in a multiplicative way. We find that the two models show highly consistent response surfaces, both indicating concave surfaces to changes in temperature and precipitation; nonetheless, the FE model

has more drastic responses to extreme climate conditions. For instance, for Sub-Saharan Africa, where climate has been extremely hot and dry, the effects of historical climate change are reported as reductions of GDP growth by 0.73 and 0.58 percentage points for the FE and IE model, respectively. On a global level, the average historical impacts of climate change on GDP growth are reported as -0.30 and -0.19 percentage points by the FE and IE model, respectively.

Summary of Author Contributions in Papers

The first paper is a collaborative work with Thomas Leirvik and Martin Wild. T.L. and I initiated and conceived the research. T.L. and M.W. provided invaluable comments and guidance as I implemented the empirical calculation. All of us contributed in writing the paper. I am the first and corresponding author of this paper.

In the second paper, I collaborated with Thomas Leirvik, Trude Storelvmo, Kari Alterskjær, Peter C.B. Phillips, and Christopher J. Smith. My contribution to the paper is that I performed data integration and technical analysis relevant to TCR estimation. I am the first and corresponding author of this paper.

The third paper is a single-author paper initiated, implemented, and written by me. In the last paper, I collaborated with Thomas Leirvik and Hande Karabiyik. T.L. and H.K. conceived and initiated the research. H.K. implemented the statistical tests and empirical estimation of the response function. I calculated historical impacts of climate change based on the estimated response function. T.L. provided significant insights in improving the model. H.K. and I wrote the paper with input from T.L. Since this project is still in progress, we have not decided yet the order of contribution.

References

- Akaike, H. (1998). Information Theory and an Extension of the Maximum Likelihood Principle. pages 199–213. Springer, New York, NY.
- Auffhammer, M., Hsiang, S., Schlenker, W., and Sobel, A. (2013). Using Weather Data and Climate Model Output in Economic Analyses of Climate Change. Technical report, National Bureau of Economic Research, Cambridge, MA.
- Auffhammer, M., Ramanathan, V., and Vincent, J. R. (2012). Climate change, the monsoon, and rice yield in India. *Climatic Change*, 111(2):411–424.
- Barreca, A., Clay, K., Deschenes, O., Greenstone, M., and Shapiro, J. S. (2016). Adapting to climate change: The remarkable decline in the US temperature-mortality relationship over the Twentieth Century. *Journal of Political Economy*, 124(1):105–159.
- Barreca, A. I. and Shimshack, J. P. (2012). Absolute humidity, temperature, and influenza mortality: 30 years of county-level evidence from the united states. *American Journal of Epidemiology*, 176(SUPPL. 7).
- Berlemann, M. and Wenzel, D. (2018). Precipitation and Economic Growth. *CESifo Working Paper No. 7258*.
- Bhargava, A., Jamison, D. T., Lau, L. J., and Murray, C. J. (2001). Modeling the effects of health on economic growth. *Journal of Health Economics*, 20(3):423–440.
- Bhatt, S., Gething, P. W., Brady, O. J., Messina, J. P., Farlow, A. W., Moyes, C. L., Drake, J. M., Brownstein, J. S., Hoen, A. G., Sankoh, O., Myers, M. F., George, D. B., Jaenisch, T., William Wint, G. R., Simmons, C. P., Scott, T. W., Farrar, J. J., and Hay, S. I. (2013). The global distribution and burden of dengue. *Nature*, 496(7446):504–507.
- Bloom, D. E., Canning, D., and Sevilla, J. (2004). The effect of health on economic growth: A production function approach. *World Development*, 32(1):1–13.
- Budyko, M. I. (1969). The effect of solar radiation variations on the climate of the Earth. *Tellus*, 21(5):611–619.
- Bureau of Meteorology (2020). Annual climate statement 2020. Technical report.
- Burke, E. J. and Brown, S. J. (2008). Evaluating uncertainties in the projection of future drought. *Journal of Hydrometeorology*, 9(2):292–299.
- Burke, E. J., Brown, S. J., and Christidis, N. (2006). Modelling the recent evolution of global drought and projections for the twenty-first century with the Hadley Centre climate model. *Journal of Hydrometeorology*, 7(5):1113–1125.
- Burke, M., Hsiang, S. M., and Miguel, E. (2015). Global non-linear effect of temperature on economic production. *Nature*, 527(7577):235–239.
- Carballar-Lejarazú, R., Ogaugwu, C., Tushar, T., Kelsey, A., Pham, T. B., Murphy, J., Schmidt, H., Lee, Y., Lanzaro, G. C., and James, A. A. (2020). Next-generation gene drive for population modification of the malaria vector mosquito, *Anopheles gambiae*. *Proceedings of the National Academy of Sciences of the United States of America*, 117(37):22805–22814.
- Carleton, T. A. and Hsiang, S. M. (2016). Social and economic impacts of climate.

REFERENCES

- Chiacchio, M. and Wild, M. (2010). Influence of NAO and clouds on long-term seasonal variations of surface solar radiation in Europe. *Journal of Geophysical Research Atmospheres*, 115(10).
- Collins, F. C. (1995). *A comparison of spatial interpolation techniques in temperature estimation*. PhD thesis, Virginia Tech.
- Craig, M., Le Sueur, D., and Snow, B. (1999). A climate-based distribution model of malaria transmission in sub-Saharan Africa.
- Dai, A. (2013). Increasing drought under global warming in observations and models. *Nature Climate Change*, 3(1):52–58.
- Deborah, M. (2008). How to discount double-counting when it counts: Some clarifications. *The British Journal for the Philosophy of Science*, Volume 59.
- Dell, M., Jones, B. F., and Olken, B. A. (2009). Temperature and income: Reconciling new cross-sectional and panel estimates. *American Economic Review*, 99(2):198–204.
- Dell, M., Jones, B. F., and Olken, B. A. (2012). Temperature shocks and economic growth: Evidence from the last half century. *American Economic Journal: Macroeconomics*, 4(3):66–95.
- Deschenes, O. (2014a). Temperature, human health, and adaptation: A review of the empirical literature. *Energy Economics*, 46:606–619.
- Deschenes, O. (2014b). Temperature, human health, and adaptation: A review of the empirical literature. *Energy Economics*, 46:606–619.
- Diffenbaugh, N. S. and Burke, M. (2019). Global warming has increased global economic inequality. *Proceedings of the National Academy of Sciences of the United States of America*, 116(20):9808–9813.
- Duan, Y., Kumar, S., and Kinter, J. L. (2021). Evaluation of Long-term Temperature Trend and Variability in CMIP6 Multimodel Ensemble. *Geophysical Research Letters*, page e2021GL093227.
- Erxleben, J., Elder, K., and Davis, R. (2002). Comparison of spatial interpolation methods for estimating snow distribution in the Colorado Rocky Mountains. *Hydrological Processes*, 16(18):3627–3649. <https://doi.org/10.1002/hyp.1239>.
- Eyring, V., Bony, S., Meehl, G. A., Senior, C. A., Stevens, B., Stouffer, R. J., and Taylor, K. E. (2016). Overview of the Coupled Model Intercomparison Project Phase 6 (CMIP6) experimental design and organization. *Geoscientific Model Development*, 9(5):1937–1958.
- Flato, G. and Marotzke, J. (2013). *Evaluation of Climate Models*. Cambridge University Press.
- Gerten, D., Rost, S., von Bloh, W., and Lucht, W. (2008). Causes of change in 20th century global river discharge. *Geophysical Research Letters*, 35(20):20405.
- Gething, P. W., Smith, D. L., Patil, A. P., Tatem, A. J., Snow, R. W., and Hay, S. I. (2010). Climate change and the global malaria recession. *Nature*, 465(7296):342–345.
- Gething, P. W., Van Boeckel, T. P., Smith, D. L., Guerra, C. A., Patil, A. P., Snow, R. W., and Hay, S. I. (2011). Modelling the global constraints of temperature on transmission of *Plasmodium falciparum* and *P. vivax*. *Parasites and Vectors*, 4(1):1–11.
- Hansen, B. (2019). *Econometrics*.
- Harris, I., Osborn, T. J., Jones, P., and Lister, D. (2020). Version 4 of the CRU TS monthly high-resolution gridded multivariate climate dataset. *Scientific Data*, 7(1).

- Hitchcock, C. and Sober, E. (2004). Prediction versus Accommodation and the Risk of Overfitting. *The British Journal for the Philosophy of Science*, 55(1):1–34.
- Ivinson, A. J. (2002). Macroeconomics and Health: Investing in Health for Economic Development. *Nature Medicine*, 8(6):551–552.
- Jiang, Y. (2008). Prediction of monthly mean daily diffuse solar radiation using artificial neural networks and comparison with other empirical models. *Energy Policy*, 36(10):3833–3837. <https://doi.org/10.1016/J.ENPOL.2008.06.030>.
- Jones, P., Hulme, M., Briffa, K., Jones, C., Mitchell, J., and Murphy, J. (1996). Summer moisture variability over Europe in the Hadley Centre GCM using the Palmer Drought Severity Index. *International Journal of Climatology*, 16(2):155–172.
- Kucharik, C. J. and Serbin, S. P. (2008). Impacts of recent climate change on Wisconsin corn and soybean yield trends. *Environmental Research Letters*, 3(3):34003.
- Kukul, M. S. and Irmak, S. (2018). Climate-Driven Crop Yield and Yield Variability and Climate Change Impacts on the U.S. Great Plains Agricultural Production. *Scientific Reports*, 8(1):1–18.
- Leirvik, T. and Yuan, M. (2021). A Machine Learning Technique for Spatial Interpolation of Solar Radiation Observations. *Earth and Space Science*, 8(4):e2020EA001527.
- Lewis, N. S. (2016). Research opportunities to advance solar energy utilization. *Science*, 351(6271):aad1920.
- Lobell, D. B. and Burke, M. B. (2008). Why are agricultural impacts of climate change so uncertain? the importance of temperature relative to precipitation. *Environmental Research Letters*, 3(3):034007.
- Norris, J. R. and Wild, M. (2007). Trends in aerosol radiative effects over Europe inferred from observed cloud cover, solar "dimming," and solar "brightening". *Journal of Geophysical Research Atmospheres*, 112(8).
- Obryk, M. K., Fountain, A. G., Doran, P. T., Lyons, W. B., and Eastman, R. (2018). Drivers of solar radiation variability in the McMurdo Dry Valleys, Antarctica. *Scientific Reports*, 8(1):5002.
- Paaijmans, K. P., Blanford, S., Chan, B. H., and Thomas, M. B. (2012). Warmer temperatures reduce the vectorial capacity of malaria mosquitoes. *Biology Letters*, 8(3):465–468.
- Phillips, P. C., Leirvik, T., and Storelvmo, T. (2020). Econometric estimates of Earth's transient climate sensitivity. *Journal of Econometrics*, 214(1):6–32.
- Popper, K. R. K. R. and Notturmo, M. A. (1994). *The myth of the framework : in defence of science and rationality*. Routledge.
- Rind, D., Goldberg, R., Hansen, J., Rosenzweig, C., and Ruedy, R. (1990). Potential evapotranspiration and the likelihood of future drought. *Journal of Geophysical Research*, 95(D7):9983–10004.
- Sanchez-Lorenzo, A., Wild, M., Brunetti, M., Guijarro, J. A., Hakuba, M. Z., Calbó, J., Mystakidis, S., and Bartok, B. (2015). Reassessment and update of long-term trends in downward surface shortwave radiation over Europe (1939–2012). *Journal of Geophysical Research*, 120(18):9555–9569.
- Scafetta, N. and West, B. J. (2005). Estimated solar contribution to the global surface warming using the ACRIM TSI satellite composite. *Geophysical Research Letters*, 32(18):1–4.

REFERENCES

- Schlenker, W., Hanemann, W. M., and Fisher, A. C. (2005). Will U.S. Agriculture Really Benefit from Global Warming? Accounting for Irrigation in the Hedonic Approach on JSTOR. *The American Economic Review*, 95(1):395–406.
- Schlenker, W. and Lobell, D. B. (2010). Robust negative impacts of climate change on African agriculture. *Environmental Research Letters*, 5(1):014010.
- Scudellari, M. (2019). Self-destructing mosquitoes and sterilized rodents: the promise of gene drives.
- Scudiero, E., Corwin, D. L., Morari, F., Anderson, R. G., and Skaggs, T. H. (2016). Spatial interpolation quality assessment for soil sensor transect datasets. *Computers and Electronics in Agriculture*, 123:74–79. <https://doi.org/10.1016/J.COMPAG.2016.02.016>.
- Seppanen, O., Fisk, W. J., and Faulkner, D. (2003). Cost benefit analysis of the night-time ventilative cooling in office building.
- Shapiro, L. L., Whitehead, S. A., and Thomas, M. B. (2017). Quantifying the effects of temperature on mosquito and parasite traits that determine the transmission potential of human malaria. *PLoS Biology*, 15(10):e2003489.
- Stjern, C. W., Kristjánsson, J. E., and Hansen, A. W. (2009). Global dimming and global brightening - An analysis of surface radiation and cloud cover data in northern Europe. *International Journal of Climatology*, 29(5):643–653.
- Storelvmo, T., Leirvik, T., Lohmann, U., Phillips, P. C. B., and Wild, M. (2016). Disentangling greenhouse warming and aerosol cooling to reveal Earth’s climate sensitivity. *Nature Geoscience*, 9(4):286–289.
- Sun, H., Gui, D., Yan, B., Liu, Y., Liao, W., Zhu, Y., Lu, C., and Zhao, N. (2016). Assessing the potential of random forest method for estimating solar radiation using air pollution index. *Energy Conversion and Management*, 119:121 – 129. <https://doi.org/10.1016/j.enconman.2016.04.051>.
- Wang, K. and Dickinson, R. E. (2013). Contribution of solar radiation to decadal temperature variability over land. *Proceedings of the National Academy of Sciences of the United States of America*, 110(37):14877–14882.
- WDI (2020). World Development Indicators.
- Wild, M. (2009). Global dimming and brightening: A review. *Journal of Geophysical Research*, 114(D10):D00D16.
- Wild, M., Ohmura, A., Schär, C., Müller, G., Folini, D., Schwarz, M., Zytka, M., and Sanchez-Lorenzo, A. (2017). The Global Energy Balance Archive (GEBA) version 2017: A database for worldwide measured surface energy fluxes. *Earth System Science Data*, 9(2):601–613.
- Zhou, Q., Flores, A., Glenn, N. F., Walters, R., and Han, B. (2017). A machine learning approach to estimation of downward solar radiation from satellite-derived data products: An application over a semi-arid ecosystem in the us. *PloS one*, 12(8):e0180239. <https://doi.org/10.1371/journal.pone.0180239>.

CHAPTER 2

Global Trends in Downward Surface Solar Radiation from Spatial Interpolated Ground Observations during 1961-2019¹

Collaborative Paper with Thomas Leirvik¹ and Martin Wild²

¹ *Nord University Business School, Norway*

² *Institute for Atmospheric and Climate Science, ETH Zurich, Zürich, Switzerland*

Abstract

Downward surface solar radiation (SSR) is a crucial component of the Global Energy Balance, affecting temperature and the hydrological cycle profoundly, and it provides crucial information about climate change. Many studies have examined SSR trends, however they are often concentrated on specific regions due to the limited spatial coverage of ground based observation stations. To overcome the spatial limitation, this study performs a spatial interpolation based on a machine learning method, Random Forest, to interpolate monthly SSR using a number of climatic variables (e.g., various temperature indices, cloud coverage), time point indicators (the year and month of an SSR record), and coordinates of locations (latitude and longitude of the SSR record).

The predictors that provide the largest explanatory power for monthly SSR are monthly maximum temperature and month of the interpolation (representative for the TOA insolation conditions). The output of the spatial interpolation is a $0.5^\circ \times 0.5^\circ$ monthly gridded dataset with complete land coverage over the period 1961-2019, which is used afterwards in a comprehensive trend analysis for *i*) each continent separately, and *ii*) the entire globe.

¹Paper submitted to *Journal of Climate*. Revision & Resubmit.

The continental level analysis reveals the major contributors for the global dimming and brightening. In particular, the global dimming is primarily dominated by negative trends in Asia and North America; whereas Europe and Africa, as a matter of fact, have shown significant increases in SSR over the dimming period 1961-1984. Over the brightening period 1985-2019, Europe and Oceania are the largest two contributors.

2.1 Introduction

Surface solar radiation is a crucial climate variable and a main constitute of the Global Energy Balance, playing an important role in temperature change and the hydrological cycle (e.g., [Budyko, 1969](#); [Pfeifroth et al., 2018](#); [Obryk et al., 2018](#)). The positive trend in downward surface solar radiation since the 1980s in combination with increasing greenhouse gases lead to an intensification of the land-based hydrological cycle ([Wild et al., 2008](#); [Wild and Liepert, 2010](#); [Wild, 2016](#)). Moreover, it has profound impacts on various aspects of society and economy, especially on agriculture. For example, crop yields could be significantly influenced not only by increases or decreases of solar radiation through enhancing or weakening of photosynthesis, a so-called “insolation effect”, but also indirectly by the resulting temperature change from solar radiation variations ([Greenwald et al., 2006](#); [Roderick and Farquhar, 2012](#); [Gupta et al., 2017](#); [Proctor et al., 2018](#)).

To analyze the drivers and economic impact of climate change, it is of critical importance to have an understanding of surface solar radiation (hereafter referred to as SSR), in terms of its trends, levels, and variations. Ground-based observations are believed to be the most reliable long-term data source for solar radiation, and have been used in many climate studies to monitor its evolution (e.g., [Wild et al., 2005](#); [Sanchez-Lorenzo et al., 2015, 2017](#); [Pfeifroth et al., 2018](#)). SSR is a key driver of climate, and observations have been applied to study its effect on temperature (e.g. [Storelvmo et al., 2016](#); [Phillips et al., 2020](#)). Despite their reliability as compared to other sources, one of the main drawbacks of ground-based measurements is their limited temporal and spatial coverage. For a start, extensive SSR observations have a relatively short history of only multiple decades; they were not widely available until the 1960s and have a time lag

effect due to the time-consuming process of data collecting and homogenizing. Moreover, continuity of observed time series is often interrupted by missing values in observational stations due to device failure and operational malfunction. As for spatial coverage, climate stations tend to be concentrated in developed regions which can provide the financial and technical support to maintain the devices. They also tend to cluster on flat terrain rather than mountainous areas where it could be hard to establish stations in the first place. For areas with sparse station coverage, the available observations from the stations might not be sufficient to represent the overall trend over the areas. Therefore it is essential to extrapolate the available observations, in the dimension of both space and time, thereby enabling a more comprehensive overview, which better represents all areas with continuous time series. The method that aims to fill gaps in spatial datasets is called spatial interpolation. Conventional spatial interpolation methods such as Inverse Distance Weighting, Kriging, splines, etc., have seen extensive applications in various climate processes (e.g., [Collins, 1995](#); [Erxleben et al., 2002](#); [Scudiero et al., 2016](#)). This study contributes to, and expands, the existing literature by applying a novel machine learning method to interpolate a station observation dataset of SSR.

Machine learning methods have seen an increasing number of applications in spatial interpolation and shown effectiveness in reproducing and predicting climate variables with high accuracy and low uncertainty (see e.g., [Jiang, 2008](#); [Sun et al., 2016](#); [Zhou et al., 2017](#)). [Qin et al. \(2019\)](#) compared the performance of four physically deterministic models with eight machine learning models in an application of reproducing data of a certain type of radiation and reported outperformance of the machine learning methods. Existing literature are mostly focused on simulating regional patterns of climate variables, for example, [Zhou et al.](#) focus on the US whereas [Qin et al.](#) focus on China. In this study we aim for a comprehensive study of SSR on a global scale; therefore, it is essential that the selected method should be able to cope with a large quantity of data. Among a wide range of machine learning approaches, *Random Forest* has exceptional advantages in handling a large number of explanatory variables and in its capacity of processing large datasets due to its computational efficiency ([Firth et al., 2005](#); [Myoung et al., 2020](#)). The study of [Leirvik and Yuan](#)

(2020) compared the performance of Random Forest with those of seven other conventional (deterministic) spatial interpolation methods (e.g., linear regression models, Kriging, Regression Kriging) in an application of predicting global SSR, and showed a profound advantage of Random Forest in prediction accuracy and performance stability. In their application they also investigated the potential of other machine learning models (i.e., *support vector machine* and *gradient boosting machine*), but they found it is hard for other machine learning methods to converge in the specific application given the global scale of the input dataset and the large number of explanatory variables. Due to the superior performance of the Random Forest method in the settings described above, which is similar to the setting in this paper, we choose to apply the Random Forest model to unsampled areas, thereby constructing a global, and more complete, dataset than has been constructed before.

In this paper, we apply Random Forest to a global SSR dataset, the dataset of the Global Energy Balance Archive (GEBA). A total of 15 variables are selected as predictors for SSR, including 9 climatic variables (various temperature indices, cloud cover, frost days, etc.), geographical coordinates (i.e., longitude and latitude), altitude, urbanization and temporal indicators that indicate the time point (year and month) of the observed/simulated SSR record. The model is first trained on available observations in the dataset (with global average R squared and mean absolute error being 0.91 and 11.86 Wm^{-2} , respectively), and then the model is applied to interpolate values at unsampled locations. The result is a $0.5^\circ \times 0.5^\circ$ monthly gridded dataset, conforming with the resolution and time step of the input CRU dataset. The constructed dataset provides SSR estimations with complete global land coverage and temporal coverage of 59 years (1961-2019). Based on this dataset, remote land areas, such as Africa, Siberia, etc., that were barely investigated before, are made accessible for investigation of their long-term trends.

Trends could vary, or even reverse, during a multidecadal time period, making it highly important to detect potential breakpoints over the whole period. In fact, not only are the long-term trends reaching far back in the past of interest, it is also of critical importance to identify the most recent sustainable trends up until now. Particularly, global SSR experiences a widespread reduction (on

the order of $3 - 9 \text{ Wm}^{-2}$ per decade) from the 1950s to the 1980s and followed by an increase (on the order of $1 - 4 \text{ Wm}^{-2}$ per decade), which are referred to as “global dimming” and “global brightening”, respectively (Wild et al., 2005; Wild, 2009; Gilgen et al., 2009; Wild, 2012; Pfeifroth et al., 2018). Aggregated series over a region reveal the overall inter-annual variation and trends, but sub-regional trends are neutralized, or masked, by the aggregation if they are of opposite sign, which is often the case in many continents. Therefore, the spatial distribution is investigated for each continent in this study, and the results show significant spatial diversity.

The paper is organized as follows: section 2 describes the datasets and methods used in the spatial interpolation; model performance and trend analyses based on the constructed dataset are discussed in section 3; section 4 is a discussion of the results found in the paper.

2.2 Datasets and Method

2.2.1 Method

Random Forest (RF) is a decision tree technique for regression and classification (Breiman, 2001). In contrast to conventional decision tree methods, Random Forest constructs a forest of decision trees that operates as a predicting ensemble whose prediction accuracy is higher than that of any individual tree. Randomness in the RF is the distinctive characteristic that makes it one of the most powerful and widely-used machine learning methods in recent applications (Sun et al., 2016; Zhou et al., 2017; Xu et al., 2018).

There are mainly two sources of this randomness. Firstly, the RF uses bootstrap to generate training sets for each decision tree which allows for replacement. The process is often known as bagging; it helps to improve the performance stability by reducing variance and avoiding over-fitting in the algorithm. Secondly, it incorporates feature randomness in that each tree in the forest corresponds to only a random subset of independent variables. This adds more diversity in the trees, resulting in a higher utilization for various regressors in parallel, rather than splitting at the most separation among observations sequentially in one decision tree. The parameters that control the two types

of randomness are the number of bootstraps (i.e., the number of independent samples used to train the model) and the degree of feature randomness (i.e., the number of candidate independent variables to split at in each node). Through a parameter tuning process the number of bootstraps is set to 700 and the degree of feature randomness is set to 8 (see Supporting Information (SI) [A.3.1](#) for details).

A range of variables are used as predictors for SSR, including climatic variables that are closely related to the variation of SSR, geographical characteristics of locations, together with temporal stamps of the records. Table [2.1](#) summarizes the symbols and detailed definition of the predictors.

Table 2.1 Predictors summary

Variable Category	Symbol	Definition
Climatic Variables	cld	cloud cover as percentage
	dtr	diurnal temperature range in $^{\circ}C$
	frs	number of days with ground frost
	pre	monthly total precipitation data in mm/month
	tmn	minimum temperature in $^{\circ}C$
	tmp	mean temperature in $^{\circ}C$
	tmx	maximum temperature in $^{\circ}C$
	wet	number of rainy days in a month
Geographical Variables	lat	latitude of the location
	lon	longitude of the location
	alt	terrain altitude in m
Temporal Variables	urban	1 if urban, 0 if rural
	year	year of the observation/estimation
	mon	month of the observation/estimation

Three error metrics are calculated for model evaluation: Mean Absolute Error (MAE), Root Mean Squared Error (RMSE), and R squared (R^2). They are given by the following equations:

$$\begin{aligned}
MAE &= \frac{1}{n} \sum_{i=1}^n |\hat{z}_i - z_i| \\
RMSE &= \sqrt{\frac{1}{n} \sum_{i=1}^n (\hat{z}_i - z_i)^2} \\
R^2 &= 1 - \frac{\sum_{i=1}^n (\hat{z}_i - z_i)^2}{\sum_{i=1}^n (z_i - \bar{z}_i)^2}
\end{aligned} \tag{2.1}$$

where n is the number of predictions, \hat{z}_i is the predicted value of station i , and z_i is the observed value of station i . No percentage error measure is used in the paper because it could be biased toward very large values by small observation values close to zero, which are common in winter.

2.2.2 Datasets

Ground-based all-sky SSR observations were obtained from the Global Energy Balance Archive (GEBA, [Wild et al. \(2017\)](#)). The GEBA dataset contains monthly SSR values from around 1500 observation stations scattered on all continents except for Antarctica. Table 2.2 provides a summary of the number of stations and monthly observations in each station. Europe accounts for more than one-third of the global stations, making it the most extensively covered continent (refer to SI [Figure A.1](#) for a global station distribution map). The dataset has an unparalleled temporal coverage, which starts from the early 1950s until 2013. This dataset has been previously examined for temporal homogeneity by [Sanchez-Lorenzo et al. \(2013\)](#) and widely used in the literature since the 1990s (see e.g., [Ohmura and Gilgen \(1993\)](#); [Arking \(1996\)](#); [Nabat et al. \(2014\)](#); [Wang et al. \(2014\)](#); [Cherian et al. \(2014\)](#); [He et al. \(2018\)](#)).

The climatic variables as predictors for SSR are available from the Climate Research Unit Time-series data version 4.04 (CRU-TS v.4.04, [Harris et al. \(2020\)](#)). The CRU dataset provides high resolution ($0.5^\circ \times 0.5^\circ$) gridded data of monthly observations for a range of meteorological variables over the period 1901-2019 (Table 2.1). A $0.5^\circ \times 0.5^\circ$ global altitude map is available from [NESDIS \(1995\)](#). The GRUMP dataset (V1) ([CIESIN, 2004](#)) provides a 30 arc-second urban extents grid based on 1995 data for all land areas except Antarctica and parts of the Greenland ice sheet. Each grid is classified as either rural or urban.

Table 2.2 Number of stations and observations in each continent

Continent	Abbr. ^a	# of stations ^b	# of obs. ^c
South America	SA	134	13,362
Oceania	OC	76	13,549
Africa	AF	234	33,238
North America	NrA	214	37,427
Asia	AS	312	98,912
Europe	EU	516	131,734
Total		1486	328,222

^a Abbreviation for continent names.

^b Number of stations in the continent.

^c Number of monthly observations in the continent.

In order to merge the GRUMP with the CRU data, each $0.5^\circ \times 0.5^\circ$ grid cell was obtained as the mean of the 3600 GRUMP values contained in the cell.

The training dataset is obtained by co-locating the GEBA stations with corresponding gridboxes in the gridded datasets, such that for each station in the GEBA a range of predictor variables as well as the SSR values are matched by month. Limited by the data availability in the GEBA dataset, the training dataset covers the period from 1961 until 2013. For interpolation, all three gridded datasets are merged and provide the input variables for the trained RF model. The interpolation data covers the period from 1961-2019, with the end year given by the extension of the CRU dataset.

2.3 Results

2.3.1 Estimation and Evaluation

A continent-by-continent 10-fold cross validation (CV) was implemented on the training dataset, such that each continent's distinctive characteristics is sufficiently accounted for. Otherwise, if a global universal model is trained, the trained model would be biased towards the SSR dynamics of the continent with the most concentrated observations, i.e., Europe. 10-fold CV means to partition the training dataset into 10 equal size subsamples. Of the 10 subsamples, a single subsample is retained as the validation data for testing the model, and

the remaining 9 subsamples are used as the data to train the model. The cross-validation is repeated 10 times, such that each of the 10 subsamples is used once as validation data. Combining together simulations for all 10 validation subsets generates a complete out-of-sample simulation (i.e., the data used for validation is not used in training) for each observation.

Table 2.3 shows the error measures of monthly anomalies and raw values (or unprocessed values) of SSR for each continent. In order to obtain monthly anomalies, for each station raw monthly SSR values are deseasonalized by subtracting the 1961-2013 mean for the corresponding month, or the mean over the sub-period during which the station existed/exists. Stations existing less than 15 years are excluded to alleviate bias brought from stations that only existed briefly in history. The R^2 of raw values range from the lowest 0.79 (South America) to the highest 0.97 (North America and Europe), with a global average of 0.91. This indicates that our RF model captures approximately 91% of the global SSR variation, primarily induced by the seasonal cycles. If removing seasonality from SSR, the R^2 calculated based on monthly anomalies remain to be reasonably high for Oceania, North America, Asia, and Europe, indicating the model's ability in capturing interannual variabilities of these continents; generally more than 35% of the interannual variability and nearly 50% for Europe. On the other hand, the model is not as effective in capturing interannual variabilities of SSR in South America and Africa, with R^2 of anomalies being only 0.09 and 0.11, respectively. This means that the large values of R^2 of raw values are dominated by seasonality in the two continents. The small values of R^2 based on monthly anomalies could be possibly due to either the limitation of the model's simulation capacity or the weaker interannual variability in the continents.

RF is a data-intensive machine learning approach which learns model features solely based on input data and does not rely on any presumptions about model structure or specification; the performance of which is highly dependent on the input training data, from perspectives of both quality and quantity. Note that the RF model was trained for per continent, that is, data characteristics in each continent affects its performance. Specifically, possible reasons that lead to the lower RF performance in South America and Africa include, but are not limited to, the relatively smaller amount of data available and/or the lack of

2. GLOBAL TRENDS IN DOWNWARD SURFACE SOLAR RADIATION

homogeneity in the continents' data. The scatter plots of simulations against observations (Figure 2.1) provide further graphical confirmation of this. The continents with better performance show highly clustered points alongside the regression line, in contrast to South America and Africa (Figure 2.1AB), which show more scattered points away from the regression line.

Table 2.3 Error measures for RF simulations

Continent	Anomalies			Raw
	MAE.ano	RMSE.ano	R.Squared.ano	R.Squared.raw
South America	17.97	24.40	0.09	0.79
Africa	13.62	18.42	0.11	0.87
Oceania	10.03	14.33	0.37	0.96
North America	9.29	13.33	0.39	0.97
Asia	11.84	16.67	0.39	0.92
Europe	8.42	12.95	0.49	0.97
Global Avg.	11.86	16.68	0.30	0.91

Monthly anomalies are calculated as the deviation from the 1961-2013 mean.

From the permutation variable importance analysis (Figure 2.2), we see that the most important variable in determining monthly SSR is not surprisingly *month*. The strong influence of the *month* comes from the fact that SSR has a strong seasonal cycle, at least outside the tropics, so for a prediction of SSR on a monthly basis it is essential to know which month/time of the year it is. On the other hand, the physical process behind this *month* variable would then be the varying incoming solar radiation at the Top of Atmosphere (TOA) over the course of a year (determined by astronomical factors). So one could see the *month* also as an indication of the TOA insolation at the location to be interpolated. Latitude is the third most influential indicator; it represents the spatial distribution of SSR, more specifically, SSR varies largely as latitude changes, while longitude (the 9th important indicator) makes little contribution in estimating SSR. However, while the above quantities govern the seasonal and latitudinal distribution of SSR, they do not influence the estimation of the SSR trends. These are determined by the climatic variables, among which temperature indices (i.e., *tmx*, *tmp*, *dtr*, *tmn*) and cloud coverage (*cld*) provide the most explanatory power. Particularly, monthly maximum temperature (*tmx*)

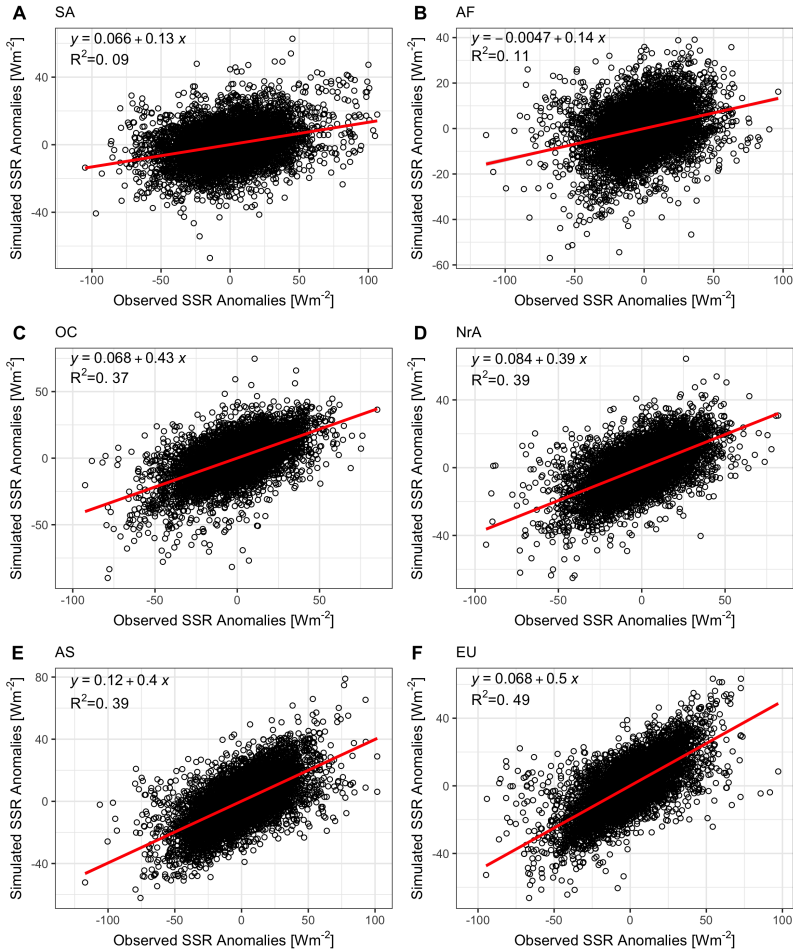


Fig. 2.1 Simulated against observed monthly anomalies. The red line is obtained by regressing simulated SSR on observed SSR, together with the corresponding equation and R squared. R^2 is the coefficient of determination of the regression. See SI [Figure A.4](#) for a scatter plot counterpart of SSR raw values.

is the second most important variable, only second to *month*. Monthly average temperature and diurnal temperature range are also important indicators for SSR trends.

2.3.2 Interpolated SSR Dataset Trend Analysis

The 10-fold cross validation (CV) shows the RF model's capability in out-of-sample estimation of SSR. In order to make use of the SSR information in

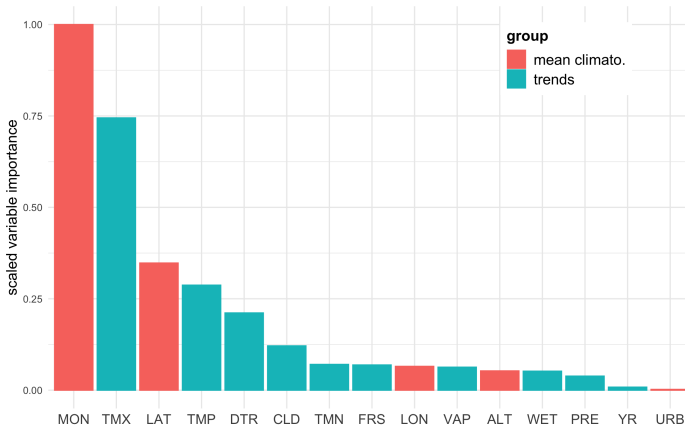


Fig. 2.2 Random Forest permutation variable importance. All importance values are scaled by the largest importance. The variables are classified into two groups: the climate variables that govern the SSR trends (in blue); and the static variables (e.g., latitude) and month (a proxy of TOA) that determine the mean climatologies of SSR and have no influence on the trends (in coral).

the GEBA dataset exhaustively, all available SSR observations (instead of 9 out of 10 subsamples used in the 10-fold CV) are used to train the RF model per continent. The trained RF models are then applied to the interpolation data. The result of the interpolation is a 0.5 by 0.5 degree gridded monthly SSR dataset over the period 1961-2019 with complete coverage over global land areas. The resolution and the time span is determined by the input climatic variables from the CRU dataset. Note that the GEBA (training) dataset has substantial amount of observations only until 2013. By extending the prediction period up until 2019, we assume the prediction relationship between SSR and the predictors remain the same for the history and onwards.

A station in the GEBA dataset—station 1188—is given as an example to illustrate the procedure. The station is located at Locarno-Monti (46.17N, 8.78E), Switzerland, and is one of the longest-standing stations in Europe. We started with the observations (shown by the red lines in Figure 2.3) from the GEBA dataset. A 10-fold CV was implemented on Europe and thereby generating out-of-sample estimations corresponding to the observations. The estimation series are shown by the black lines. Then all available data in Europe were used to train a RF model which was later used in interpolation for each

gridbox in Europe. By extracting the values in the gridbox in which station 1188 is located, interpolation series are obtained (shown by the blue lines). We see that the interpolation series approximate the observations more precisely than the simulations, this is because the interpolation is an in-sample forecast which uses 10% more data than the simulations which are based on the 10-fold CV. By comparing the blue lines with the red lines, we see that the interpolation series are able to capture the observed SSR variation with reasonable accuracy, indicating the robustness of the RF model and the reliability of the generated interpolation series.

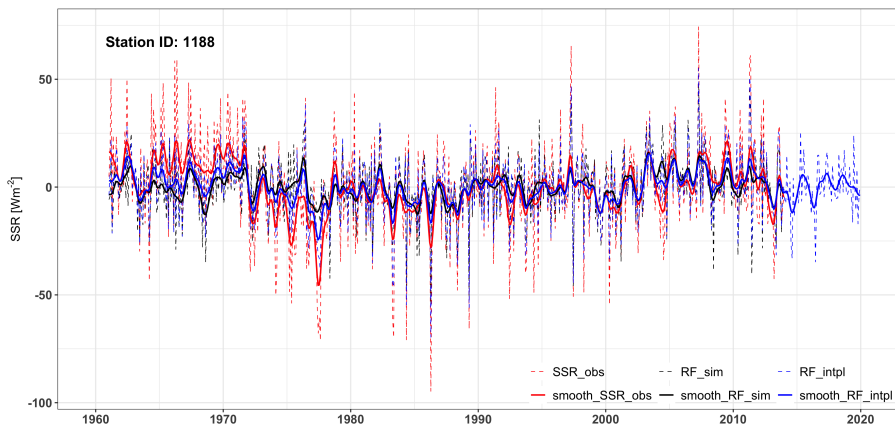


Fig. 2.3 Monthly anomalies for station 1188, Locarno-Monti, Switzerland. Monthly SSR anomaly series (dashed lines) are shown for observations (the red dashed line), simulations (the black dashed line), and interpolations (the blue dashed line), together with their corresponding smoothed series (solid lines) using 12-month Gaussian kernel. The series are expressed as anomalies from the 1961-2019 mean.

Trend Overview over the Entire Period

Annual anomalies for global land areas and for each continent are shown in Figure 2.4 and 2.5. The global average SSR exhibits rapid dimming trends from 1961 until the mid 1980s, followed by a moderate reversal. A similar reversal is observed in Oceania, North America, and South America, in contrast to the relatively continuous positive trends in Europe and Africa. Asia had a drastic dimming period from 1961 until early 1990s and the continental average SSR has been stable since then.

2. GLOBAL TRENDS IN DOWNWARD SURFACE SOLAR RADIATION

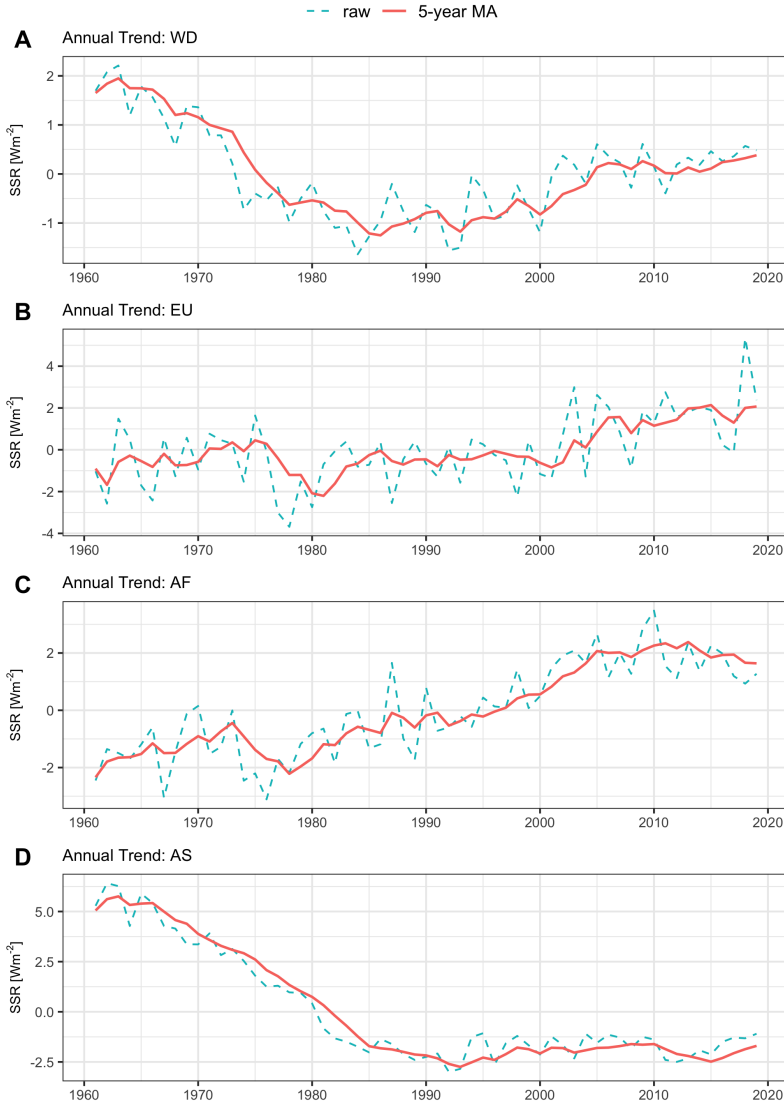


Fig. 2.4 Annual anomalies over the period 1961-2019, part I. The raw series is shown by the green dashed line, and the 5-year moving average (MA) series is shown by the coral solid line. When the number of years is less than 5, a partial moving average is used for the available years up until the time point. The anomaly series are based on the average of the period 1961-2019. Subplots show results respectively for: A-World, B-Europe, C-Africa, D-Asia. Refer to SI [Figure A.5](#)—[Figure A.8](#) for the continents' monthly anomaly figures.

Although the global trend reversal takes place at the mid 1980s, each continent shows different breakpoints, making it of interest to detect structural

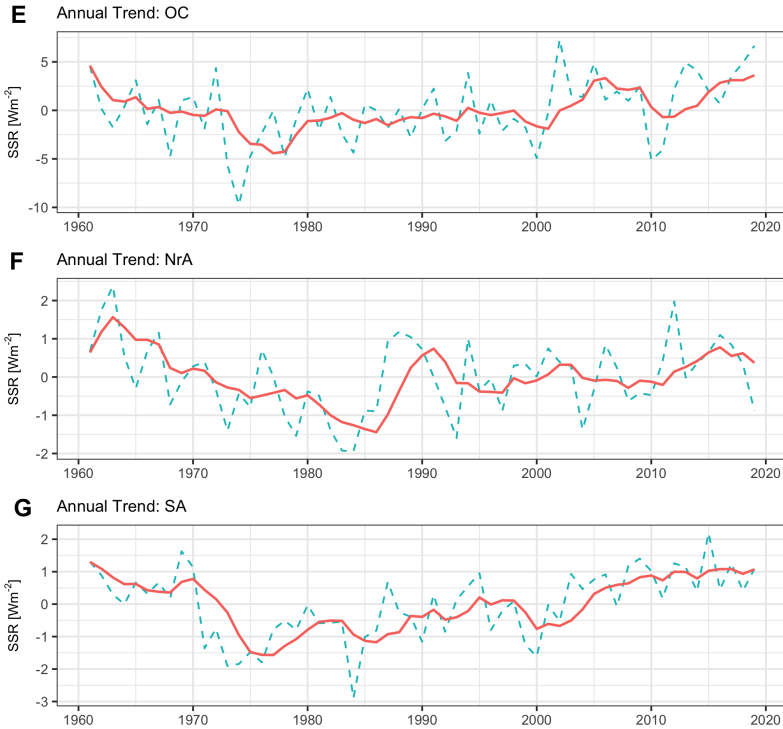


Fig. 2.5 Annual average anomalies over the period 1961-2019, part II. Refer to Figure 2.4 for the series legends. Subplots show results respectively for: E-Oceania, F-North America, G-South America. Refer to SI Figure A.9—Figure A.11 for the continents’ monthly anomaly figures.

change for each continent separately. Breakpoints were detected based on moving sums (MOSUMS) of recursive and least-squares residuals for annual mean values which, despite of losing monthly temporal details, enables an investigation of interannual variation and time series segments (Forkel et al., 2013). Time series segment and structural change detection is widely used in climate research (e.g., Cró and Martins, 2017; Adedoyin et al., 2020; Vu et al., 2019). Readers are referred to Holben (1986) and Bai and Perron (1998, 2003) for the detailed implementation of the algorithm.

Any breakpoints with the Mann-Kendall trend test significant at 5% are identified and trends over the separated segments are reported in Table 2.4. Asia and North America, with decadal linear trends being -3.07 and -1.06 Wm^{-2}/dec , respectively, are the two largest contributors to the global dimming;

whereas the global brightening is mostly attributed to the increasing trends in Africa, Europe, and Oceania. Overall, with the exception of the stagnated trends in Africa for the past decade, continents show either a trend transition from negative to neutral/positive (Asia, North America, and Oceania) or a trend strengthening from less positive to more positive (Europe, and South America). It is worth noting that except for Africa that has two breakpoints (1973 and 2010), only one breakpoint is detected for other continents. In what follows, this paper will investigate more thoroughly on periods after the latest detected breakpoints. However, since the latest breakpoint (2010) in Africa is rather recent and the period after that might not be long enough to consider its long-term trends, we will focus on the period after 1973 when Africa is referred to.

Given the large variability of SSR, the linear trends could be affected significantly by the different choices of start and end time. To avoid this bias, a running-trend estimation was implemented on the annual global average series for all possible segments equal or longer than 10 years. The global decadal trend raster (Figure 2.6) corroborates the annual anomaly series (Figure 2.4A). The most negative trends are found between 1965 and 1970 (referring to the start points), in contrast to the most positive trends over 1990-2000. After entering into the 21st century, the trends fade away. The continental running-trend rasters (Figure 2.7) show that Europe, Africa, and South America are dominated by positive trends, in contrary to Asia which is dominated by negative trends. The largest variation occurs in Oceania, where the trends span from the most negative $-5 \text{ Wm}^{-2}/\text{dec}$ in the mid 1960s to the most positive $5 \text{ Wm}^{-2}/\text{dec}$ around the mid 1990s and the early 2010s.

The results shed light on how SSR trends evolve over time; nevertheless, because the data are aggregated over areas, either globally or continentally, opposite trends cancel each other out when calculating the areal averages, resulting in less distinct trends overall. Therefore also the regional distribution of trends as resolved by the 0.5 by 0.5 degree has been investigated. In what follows, interannual variabilities of annual and seasonal SSR for the globe and each continent are discussed based on their latest detected breakpoints

Table 2.4 Decadal linear trends for annual average SSR. After significant breakpoints are detected, the linear trend of the continental average time series is estimated by least-squares for each segment. The first row for each continent or the world shows the trend over the whole period; sub-periods split by the breakpoints are shown in the following rows. For instance, the global average trend shows a negative slope of $-0.15 \text{ Wm}^{-2}/\text{dec}$ over 1961-2019 and one breakpoint at 1984 is significantly detected. Split by 1984, a negative trend of $-1.54 \text{ Wm}^{-2}/\text{dec}$ is reported over the first segment and a positive trend of $+0.49 \text{ Wm}^{-2}/\text{dec}$ is reported over the latter segment.

Continent	Segment	Slope ^a	Slope std	<i>t</i> value	Pval	Pval.symbol ^b
World	1961-2019	-0.150	0.069	-2.185	0.033	*
	1961-1984	-1.535	0.117	-13.077	0.000	***
	1985-2019	0.486	0.071	6.892	0.000	***
Europe	1961-2019	0.500 ^c	0.113	4.433	0.000	***
	1961-1976	0.921	0.701	1.313	0.210	
	1977-2019	1.010	0.161	6.258	0.000	***
Africa	1961-2019	0.760	0.072	10.520	0.000	***
	1961-1973	1.196	0.620	1.927	0.080	.
	1974-2010	1.319	0.122	10.850	0.000	***
	2011-2019	-0.564	0.679	-0.831	0.434	
Asia	1961-2019	-1.278	0.123	-10.406	0.000	***
	1961-1993	-3.074	0.112	-27.476	0.000	***
	1994-2019	-0.032	0.132	-0.244	0.810	
Oceania	1961-2019	0.638	0.244	2.614	0.011	*
	1961-1972	-0.573	2.382	-0.241	0.815	
	1973-2019	1.484	0.311	4.778	0.000	***
North America	1961-2019	0.015	0.072	0.202	0.840	
	1961-1986	-1.064	0.188	-5.667	0.000	***
	1987-2019	0.015	0.146	0.103	0.918	
South America	1961-2019	0.193	0.076	2.550	0.013	*
	1961-1970	0.284	0.611	0.466	0.654	
	1971-2019	0.547	0.072	7.568	0.000	***

^a Slope unit: Wm^{-2} per decade.

^b Significance symbol representation:

*** indicates $p < 0.001$, ** for $p < 0.01$, * for $p \leq 0.05$, . for $p \leq 0.1$, and no symbol if $p > 0.1$.

^c The linear trend is smaller than in both segments due to the large jump in 1976 (refer to panel B in Figure 2.4).

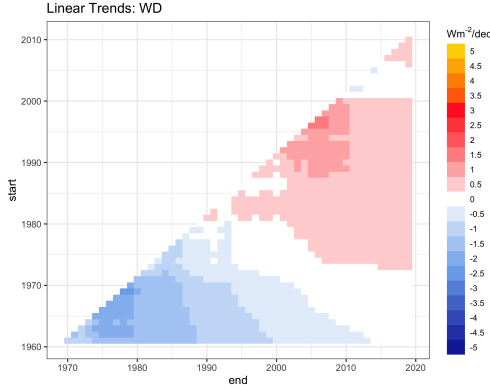


Fig. 2.6 Decadal trend raster for the global. The trends are estimated on global average SSR. The y-axis denotes the start years, and the x-axis denotes the end years.

respectively. Furthermore, the spatial distribution of the trends is visualized in annual and seasonal maps.

Latest sustainable Trend

Based on the structural breaks in trends, the latest sustainable trends, i.e., the period after the latest detected breakpoints, over the globe and each continent are inspected in this section. Their spatial and seasonal patterns are presented as trend maps for each season and the entire year. Seasons are defined as follows: winter (DJF: December-February), spring (MAM: March-May), summer (JJA: June-August), and autumn (SON: September-November). Seasonal trends after the detected breakpoints for the globe and each continent are reported in Table 2.5, which will be elaborated in the sections in what follows.

World

The global brightening starts from 1984 and continues onwards, at a moderate rate of $+0.49 \text{ Wm}^{-2}/\text{dec}$, only about one-third of the dimming rate before ($-1.54 \text{ Wm}^{-2}/\text{dec}$). Although the global average SSR has shown a positive trend since 1985, on a regional level, significant dimming is observed in certain regions, in particular eastern US, South Asia, and the Pacific island countries (Figure 2.8A). Generally, the majority of the globe has shown positive trends since 1985. Two centroids of the most positive trends globally are observed in Tibet, China, and Riyadh, Saudi Arabia, with decadal trends between 5 to 6 Wm^{-2} per decade.

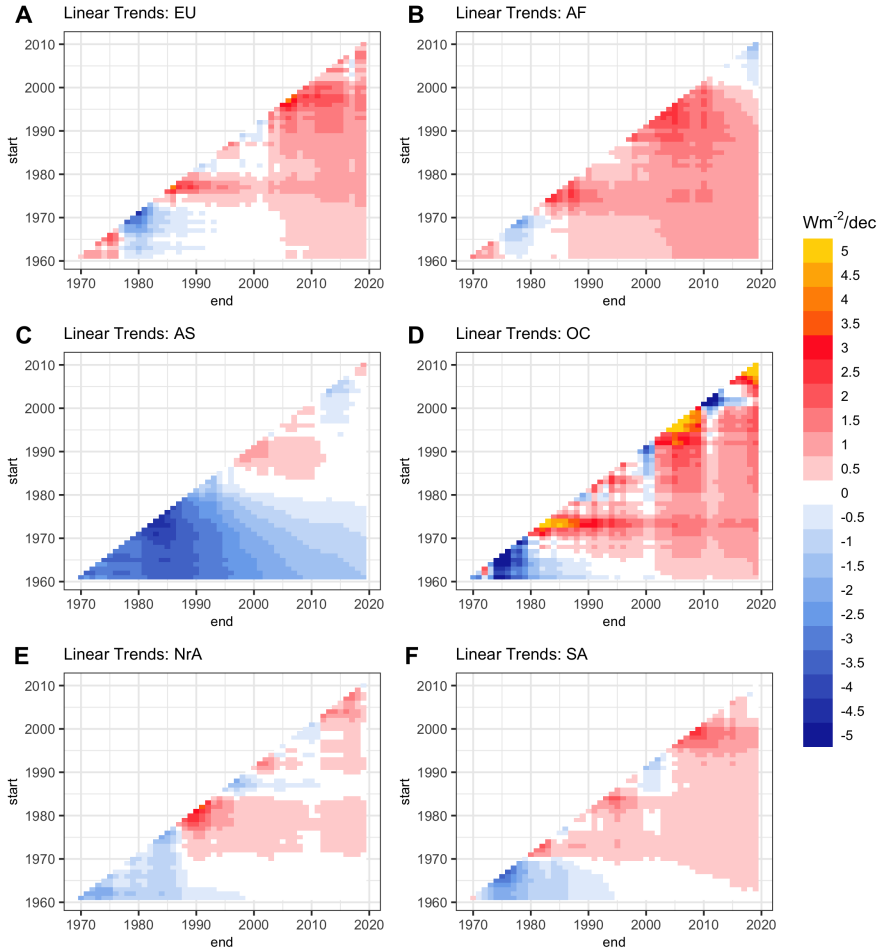


Fig. 2.7 Decadal trend rasters for continents.

The seasonal maps show that the northern hemisphere spring and summer show the largest trend variability (Figure 2.8C-D), that is, during which both the strongest positive and negative trends take place. On the other hand, northern hemispheric winter shows the modest trends, both positive and negative trends are diminished as expected due to the lower absolute SSR values in northern hemispheric winter in the extratropics. Note that the decadal trends are squeezed into a range of $-7 \sim 7 \text{ Wm}^{-2}$ per decade, namely, any extreme values falling out of the range are assigned as -7 if a value is smaller than -7 , and 7 if a value

2. GLOBAL TRENDS IN DOWNWARD SURFACE SOLAR RADIATION

Table 2.5 Decadal linear trends for seasonal average SSR over the period from the detected breakpoints until 2019.

Continent	Seasons	Slope ^a	Slope Std	<i>t</i> value	Pval	Pval.symbol ^b
World (1985-)	DJF	0.352	0.106	3.306	0.002	**
	MAM	0.609	0.120	5.087	0.000	***
	JJA	0.468	0.115	4.071	0.000	***
	SON	0.513	0.131	3.900	0.000	***
Europe (1977-)	DJF	-0.136	0.114	-1.192	0.240	
	MAM	1.318	0.333	3.956	0.000	***
	JJA	2.265	0.388	5.839	0.000	***
	SON	0.605	0.226	2.673	0.011	*
Africa (1974-)	DJF	1.031	0.177	5.838	0.000	***
	MAM	1.218	0.151	8.086	0.000	***
	JJA	0.671	0.109	6.179	0.000	***
	SON	1.038	0.129	8.047	0.000	***
Asia (1994-)	DJF	0.025	0.233	0.106	0.916	
	MAM	0.439	0.257	1.711	0.100	
	JJA	-0.273	0.261	-1.048	0.305	
	SON	-0.380	0.290	-1.312	0.202	
Oceania (1973-)	DJF	1.128	0.593	1.902	0.064	.
	MAM	1.470	0.612	2.402	0.020	*
	JJA	1.305	0.441	2.961	0.005	**
	SON	1.801	0.485	3.712	0.001	***
North America (1987-)	DJF	0.097	0.238	0.406	0.687	
	MAM	-0.375	0.250	-1.500	0.144	
	JJA	0.055	0.251	0.220	0.828	
	SON	0.304	0.313	0.972	0.339	
South America (1971-)	DJF	0.370	0.094	3.948	0.000	***
	MAM	0.480	0.134	3.574	0.001	***
	JJA	0.730	0.131	5.577	0.000	***
	SON	0.582	0.093	6.276	0.000	***

^a Slope unit: Wm^{-2} per decade.

^b Significance symbol representation: refer to Table 2.4

is larger than 7². More specifically, we observe that the positive trends over

²The 99% percentile of seasonal trends in JJA is 7.08 Wm^{-2} per decade, therefore, about 1% values larger than that are forced to be 7. As we will see in the forthcoming result (Figure 2.15), the

Tibet and Riyadh are mostly attributed to high rates in northern hemispheric spring and summer. Also noteworthy is that the dimming trends are observed throughout the year in India, with the most negative trends observed in summer. For the southern hemisphere the strongest trends are observed in winter (JJA) and spring (SON), showing widespread positive trends in general.

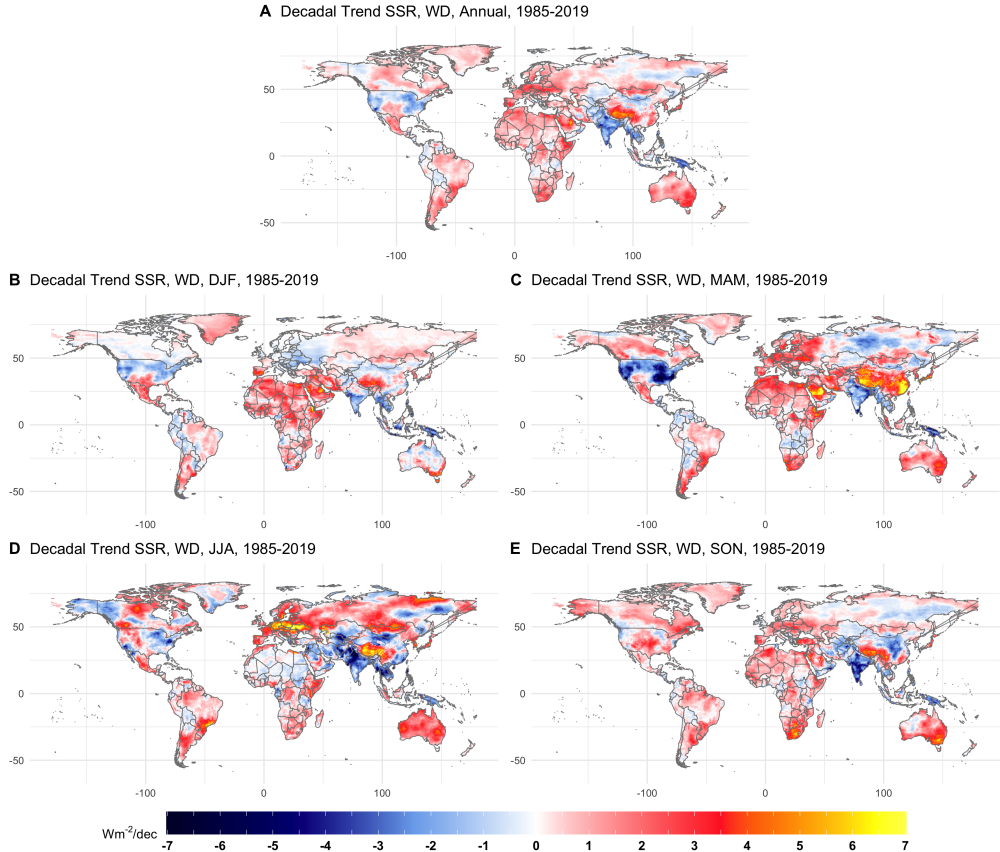


Fig. 2.8 Linear trends of the annual and seasonal average SSR over the globe during the period 1985-2019 (after the breakpoint at 1984). The values are estimated for each 0.5×0.5 degree grid and expressed as Wm^{-2} per decade. Panel A shows the decadal trends for annual average SSR. Panel B-E show the decadal trends for individual seasons. The seasons are defined as spring (MAM, dated from Mar. to May.), summer (JJA, dated from Jun. to Aug.), autumn (SON, dated from Sep. to Nov.), and winter (DJF, dated according to the year in which Jan. and Feb. belong to, plus Dec. from the previous year).

largest concentration of the trends falls within $[-4, 4] Wm^{-2}$, i.e., the upper and lower 1.5 standard deviation from the mean, making it reasonable to visualize values in a truncated range of $[-7, 7] Wm^{-2}$ per decade to better see the small absolute values.

Europe

The recent long-term trends in Europe show an increase of average SSR at the rate of $1.01 \text{ Wm}^{-2}/\text{dec}$ starting from 1977 and up until now (Table 2.4). At a seasonal scale, except for winter, all the other seasons show significant positive average trends, with summer having the strongest rate at $2.27 \text{ Wm}^{-2}/\text{dec}$ (Table 2.5).

The spatial distribution in the annual mean shows a widespread increase with the most positive area located in the Central European Domain (CED) (Figure 2.9A), defined as land areas from 45°N to 55°N and 10°W and 35°E , namely in Germany, southern Poland, Slovakia, and Ukraine. The mean annual trend for the CED is $1.81 \text{ Wm}^{-2}/\text{dec}$, which is about $0.80 \text{ Wm}^{-2}/\text{dec}$ higher than the annual trend over the whole continent. In fact, a larger difference, $2.02 \text{ Wm}^{-2}/\text{dec}$ (4.11 and $2.09 \text{ Wm}^{-2}/\text{dec}$ for decadal trends over CED and the whole EU land area, respectively), is observed if only summer (JJA) is considered. The spatial pattern is also found by [Sanchez-Lorenzo et al. \(2017\)](#), who reported higher rates of annual and seasonal SSR for the CED as compared to the entire continent. In particular, they documented a 1.0 Wm^{-2} per decade higher rate for the CED as compared to the whole continent for the annual series over the period 1983-2010, in contrast to a larger difference of $2.2 \text{ Wm}^{-2}/\text{dec}$ for the summer counterpart. It is worth noting that in summer, the trends in the Mediterranean area are actually negative, in contrary to the general positive trends over the rest of the continent. In particular, the Mediterranean area shows negative trends throughout the year except spring. The negative trends are also reported in [Sanchez-Lorenzo et al. \(2017\)](#). Furthermore, our study shows no significant European-average trends in winter; however, at a regional level, CED shows slightly negative trends, and also noteworthy are the positive trends observed in Spain and France. The continuous increase in the winter series in Spain is also reported by [Sanchez-Lorenzo et al. \(2013\)](#).

Africa

Our results show that Africa exhibits a widespread increase in SSR, especially from the 1970s to 2000s, during which the continent average SSR increases at $1.32 \text{ Wm}^{-2}/\text{dec}$ (Table 2.4, Figure 2.4C). Entering into the 2010s, the brightening trends tend to cease and no significant trends are observed. Central Africa

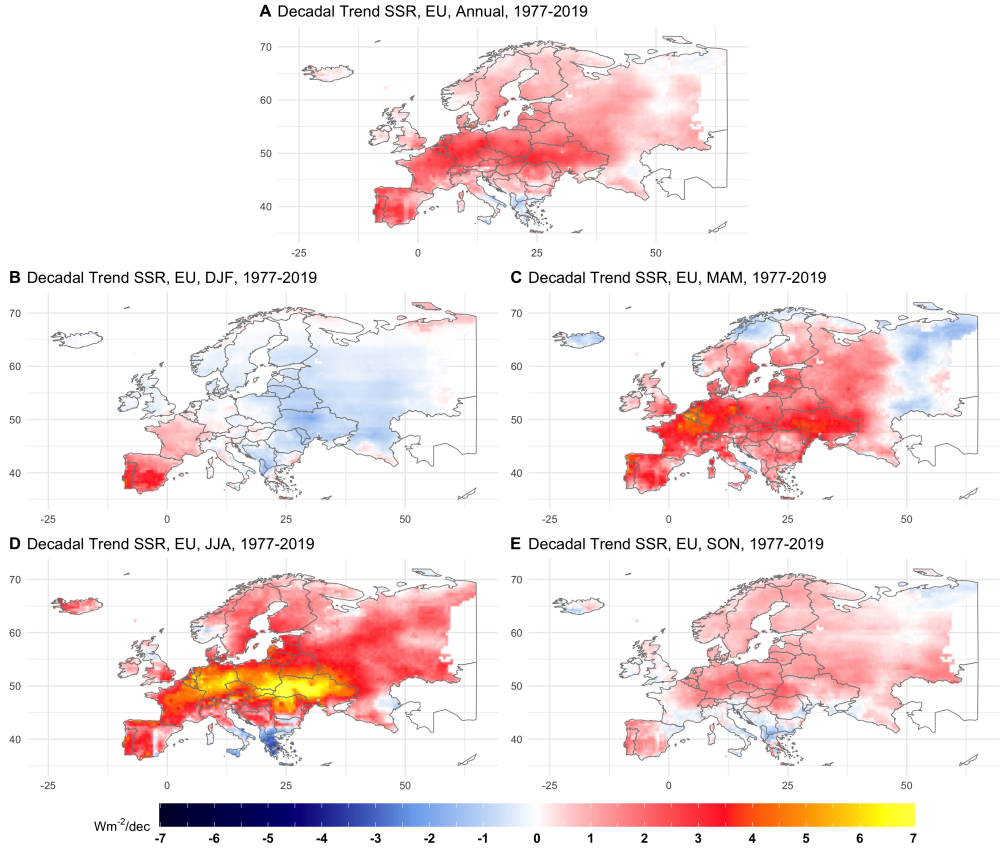


Fig. 2.9 Linear trends of the annual and seasonal average SSR in Europe during the period 1977-2019.

($20^{\circ}S \sim 20^{\circ}N$) exhibits generally weaker annual mean trends ($0.84 Wm^{-2}/dec$) as compared to the areas in the two ends (Figure 2.10A). The mean decadal trends for annual average SSR are 1.19 and $1.54 Wm^{-2}/dec$ for northern and southern Africa, respectively. This is consistent with the spatial pattern reported by Soares et al. (2019).

On the seasonal basis, all seasons show positive average trends, with the strongest rate found in northern hemispheric spring at $1.22 Wm^{-2}$ per decade (Figure 2.10B-E, Table 2.5). The weakest trends are found in northern hemispheric summer, during which equator areas show strong positive trends while Sahara area shows neutral trends.

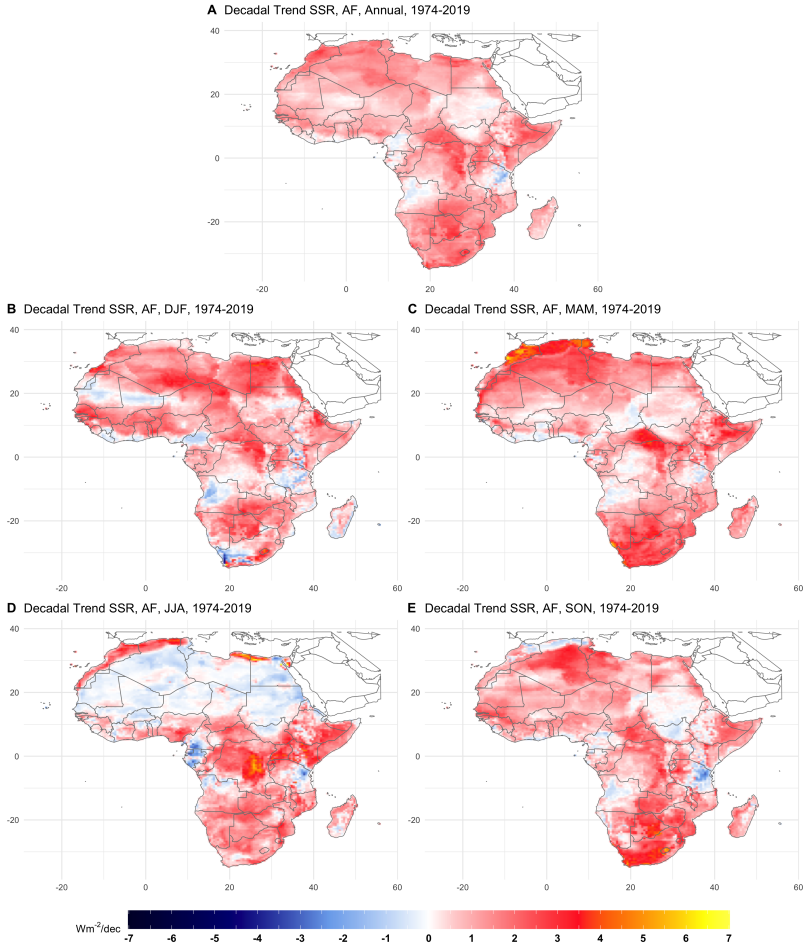


Fig. 2.10 Linear trends of the annual and seasonal average SSR in Africa during the period 1974-2019.

Asia

Large spatial variability is observed in Asia. Even though extremely strong trends exist, the opposite signs neutralize each other, resulting in insignificance in continental average trends after 1993 (Table 2.4, Figure 2.4D). On the regional level (Figure 2.11A), considerably negative trends are observed in India and Southeast Asia (consisting of countries south of China and the Pacific island countries), in contrast to the highly positive trends in the Middle East countries, Tibet, middle east of Russia, and the areas surrounding the Sea of Japan.

Generally, the negative trends over India and Southeast Asia persist throughout the year, with the most negative trends observed in summer.

On the continental scale, the most negative trends take place in autumn, with a value of $-0.38 \text{ Wm}^{-2}/\text{dec}$, while summer shows a weaker negative trend at $-0.27 \text{ Wm}^{-2}/\text{dec}$ (Table 2.5). Winter and spring show slightly positive continental average trends. Nevertheless, none of the seasonal as well as the annual continental trends are significant due to the substantial variability within the continent. The nonsignificant trends corroborate the findings by Yang et al. (2018), who indicated that the trend reversal, or jump, in the early 1990s in China is exaggerated falsely because of instrument and operational changes. A series of procedures were performed by Yang et al. to obtain a homogenized series, and based on which, they concluded that no significant trends are found in China over the period 1990-2016. Moreover, the interpolated dataset of the current paper mitigates the jump reported in the original observations by Moseid et al. (2020). This highlights that our constructed dataset functions as an adjustment to the raw observations toward a homogeneous dataset.

On a seasonal basis, two centroids of strong positive trends are identified in east China and middle Saudi Arabia in spring. In the southeastern China, trends vary largely among the seasons, more specifically, significant negative ones in autumn and winter, and substantial positive ones in spring and summer (Figure 2.11B-E).

2. GLOBAL TRENDS IN DOWNWARD SURFACE SOLAR RADIATION

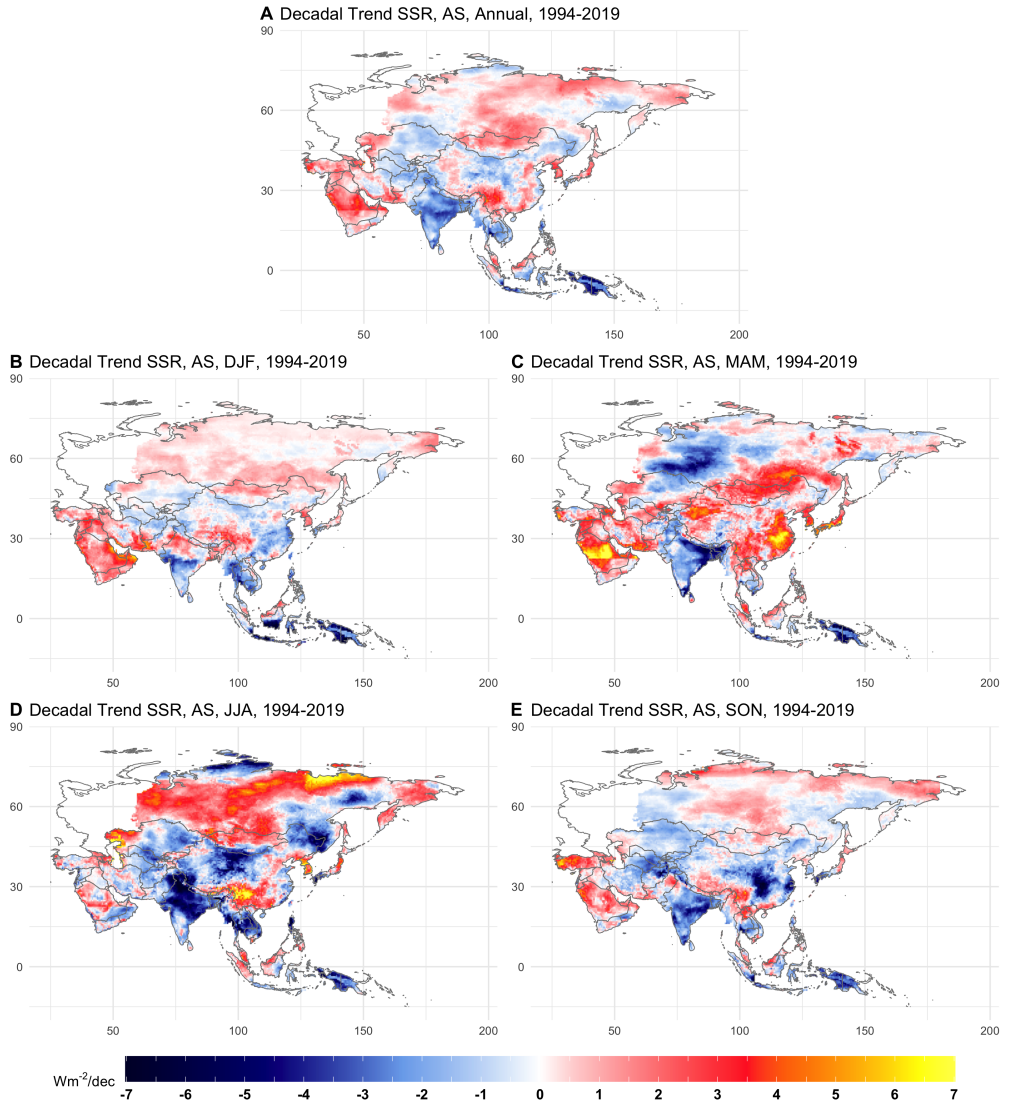


Fig. 2.11 Linear trends of the annual and seasonal average SSR in Asia during the period 1994-2019.

Oceania

Caution needs to be taken for users to interpret the historic SSR trends in Oceania prior to 1988: the original data in Australia have been artificially detrended, as the MetService there was afraid that the instruments were drifting.

Therefore, the trends prior to 1988 (Figure 2.5E) might be flatter than they are supposed to be in reality.

The latest sustainable SSR annual mean trend over Oceania is $1.48 \text{ Wm}^{-2}/\text{dec}$ starting from 1973, which is the strongest among all continents (Table 2.4, Figure 2.5E). The continent shows high extent of homogeneity (Figure 2.12). In particular, unanimous positive annual average trends are observed in Australia, with the west coast being more positive than the east coast. New Zealand shows a tendency of neutral trends. The seasonal maps show highly consistent positive trends; specifically, all seasons show positive continental average trends. The only neutral regional trends are found in the west-south coastline in summer (DJF). On a seasonal basis, the strongest continental average trend is found in spring (SON) at $1.80 \text{ Wm}^{-2}/\text{dec}$ and the weakest continental average trend is found in summer (DJF) at $1.13 \text{ Wm}^{-2}/\text{dec}$ (Table 2.5).

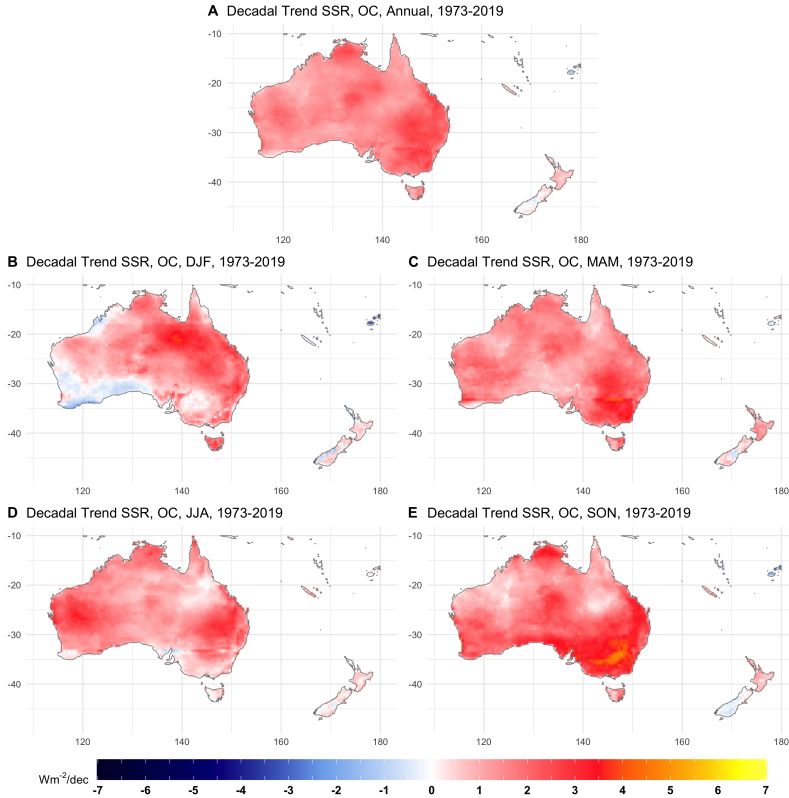


Fig. 2.12 Linear trends of the annual and seasonal average SSR in Ocean during the period 1973-2019.

North America

North America has highly diverging trends; similar to Asia, both strong positive and negative trends are observed over the period 1987-2019, resulting in the overall neutral continental average trends (Table 2.5, Figure 2.5F). Significant negative trends are observed in the eastern US in spring (Figure 2.13C). The majority of the mainland US shows generally negative trends throughout the year, except for the west-middle areas which show an increase in summer. Canada shows a tendency of positive or neutral trends throughout the year over most areas excluding the part bordering with Alaska in summer. Additionally, positive trends are also observed in Greenland and Mexico. On a seasonal basis, spring and summer show strong regional trends and winter shows the weakest trends.

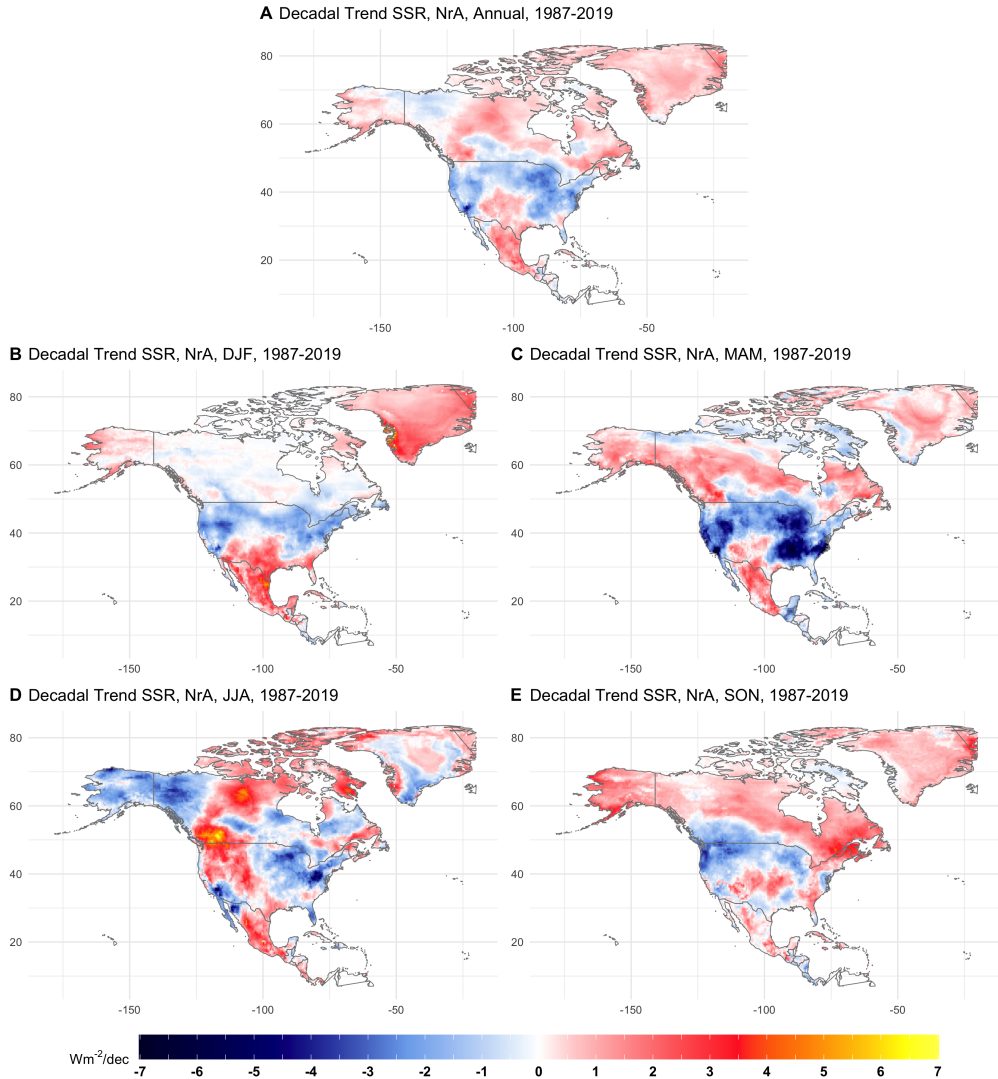


Fig. 2.13 Linear trends of the annual and seasonal average SSR in North America during the period 1987-2019.

South America

South America shows a significant and widespread increase in SSR after 1971 at an annual rate of $0.55 Wm^{-2}/dec$ (Table 2.4, Figure 2.5G). The annual average SSR trends are stronger in south (Figure 2.14A); especially in the southern region beyond $30^{\circ}S$, the annual continental trend of which is 0.60

Wm^{-2}/dec . Specifically, separated by $30^{\circ}S$, the southern region and northern region show a tendency of increase at rates 1.06 and $0.46 Wm^{-2}$ per decade, respectively. On the seasonal scale, all seasons show significant increases, with winter (JJA) having the strongest continental average trend at $0.73 Wm^{-2}/dec$, and summer (DJF) showing the weakest trend at $0.37 Wm^{-2}$ per decade (Table 2.5). The spatial distribution shows high degree of consistency among seasons.

2.4 Discussion

This study interpolates a ground-based solar radiation observation dataset and constructs a dataset with complete global land coverage at high resolution covering nearly six decades. This enables a temporal and spatial trend analysis at the continental and the regional level, making possible for the data scarce continents, e.g. Africa, to obtain a comprehensive quantification of the long-term trends. Rather than relying principally on graphic visualization, a structural breakpoint detection algorithm based on moving sums (MOSUMS test) is applied and provides quantitative identification of any structural changes in long-term series. The results show that the global dimming-brightening transition takes place around 1984, in line with existing literature based on station observations. The two divided segments show a decrease and an increase at $-1.54 Wm^{-2}$ and $+0.49 Wm^{-2}$ per decade, respectively. However, it is worth noting that on the continental level, four out of six continents, i.e., Europe, Africa, Oceania, and South America, actually show no significant decreasing trends over the entire period 1961-2019. In particular, they generally show a transition from no significant trends to positive trends (Europe, Oceania, and South America), or experience a positive trend strengthening (Africa). Therefore, it is obvious that the global dimming is attributed to the substantial reduction of SSR in Asia and North America, which show reduction rates at $-3.07 Wm^{-2}/dec$ and $-1.06 Wm^{-2}/dec$, respectively.

Over the brightening period (1985-2019), considerable spatial diversity is observed. In particular, two positive centroids are Riyadh, Saudi Arabia and Tibet, China; substantial decreasing trends are observed in the eastern US, South Asia, and the Pacific Island countries. Compared to the large spatial

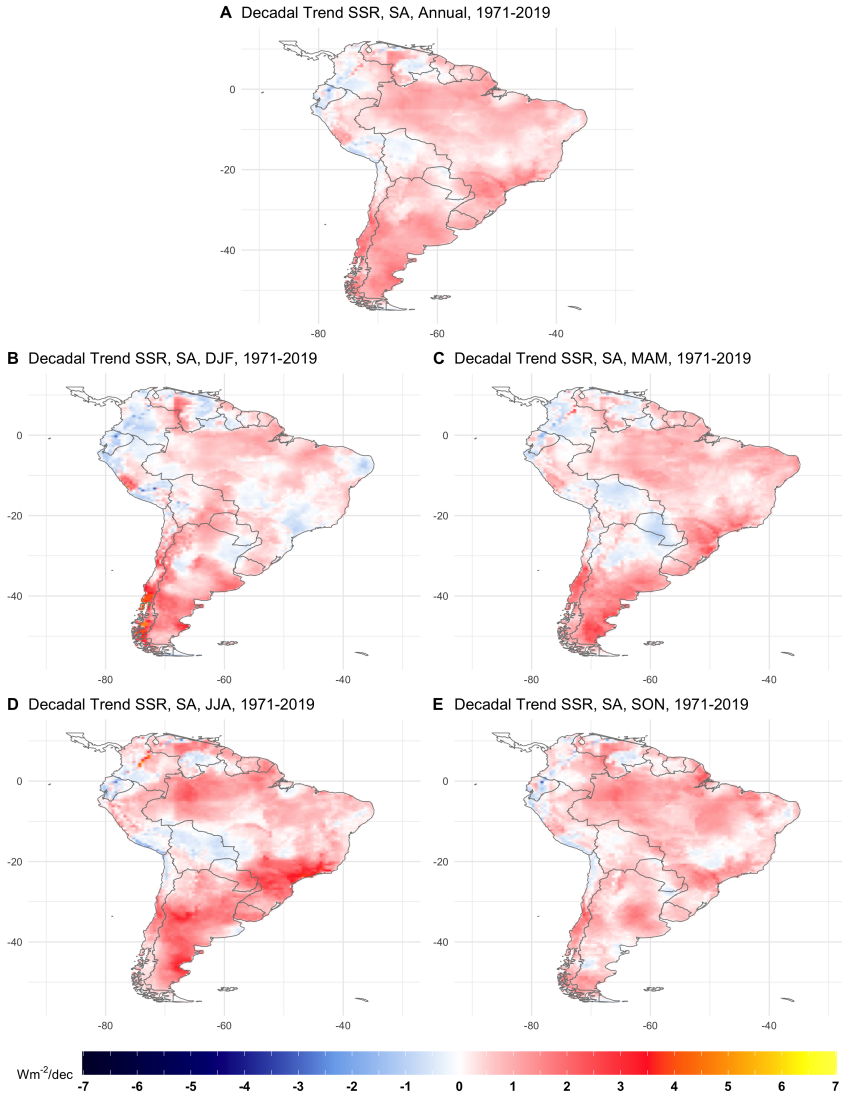


Fig. 2.14 Linear trends of the annual and seasonal average SSR in South America during the period 1971-2019.

variability in the northern hemisphere, the southern hemisphere, on the other hand, shows a consistent widespread increase.

In order to obtain an overview of the distribution of decadal trends for each gridbox within a continent, Figure 2.15 shows a box plot for annual trends as well as for each seasonal trends for all gridboxes per continent. A longer box

and a longer distance between whiskers indicate larger variability and more heterogeneity among gridboxes in a continent. We observe that most boxes are generally symmetric, that means the distribution is approximately normal. However, there exist certain boxes which are asymmetric and show skewness. For instance, the fact that the median is closer to the lower hinge shows that the winter box in North America is right skewed. In other words, the majority of trends for gridboxes are of small values, but the average trend of all gridboxes is shifted toward a larger value by certain gridboxes with strong trends. The box plots also indicate that northern hemisphere continents, i.e., Asia, North America, and Europe, show larger variability than southern hemisphere continents, which can be concluded from their wider ranges between upper and lower whisker. On a seasonal basis, the largest variability generally exists in summer, and the smallest variability exists in winter. The decadal variability for individual seasons varies largely among the continents. Specifically, box plots for South America, Africa, and Oceania are more truncated and more consistent among various seasons. In other words, decadal variabilities in southern hemisphere continents are at approximately the same level among all seasons.

The intra-annual variability is largely determined by clouds, but the longer term (decadal) variabilities are often more governed by aerosol changes (Wild, 2016; Boers et al., 2017; Pfeifroth et al., 2018). Wild et al. (2021) reported that the major cause of the brightening in Europe, especially in the Central Europe Domain, is highly affected by the aerosol effects through a reduction in anthropogenic aerosol emissions after the 1980s. Moreover, Sanchez-Lorenzo et al. (2017) found that seasonal variability of solar radiation trends in Europe is closely related to changes in cloud coverage. For example, the high rates of brightening in spring are accompanied with large rates of decrease in cloud cover; however, the strong trends in summer are less substantiated by cloud cover changes, which, in fact, demonstrate slightly positive trends. Based on the reported evidence, we speculate that the profound positive summer trends in Europe could be due to the reduction of pollution aerosols in summer (Panel EU in Figure 2.15).

This study provides an observation based dataset with complete spatial and temporal coverage. It completes the global surface solar radiation trend analysis

by analyzing continents which are rarely examined before. The quantification of long-term trends is of significant importance to solar energy deployment (Müller et al., 2014). Last but not least, this study has the potential to be used for comparison with climate model simulations. It could serve as a benchmark reference to the evaluation and calibration for global or regional climate models. Other potential applications could be climate change monitoring and a strengthened understanding of its closely related atmospheric or hydrological processes, for instance, temperature changes, aerosol dispersion, etc.

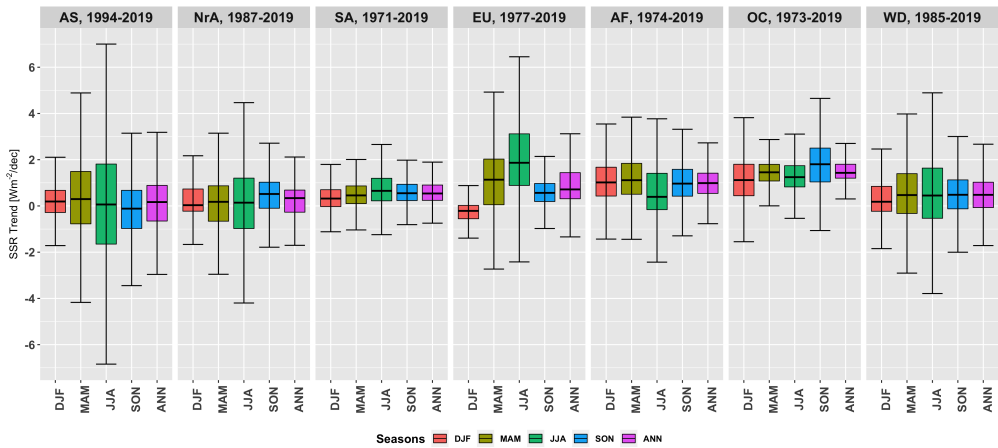


Fig. 2.15 Box plot for seasonal and annual SSR Trends. The box plots are statistics calculated based on trends at all individual gridboxes for each continent over the period after the last corresponding breakpoint and up until 2019. Five values are shown for each box plot from bottom to top: lower whisker, first quartile (Q_1), median (Q_2), third quartile (Q_3), and upper whisker. The upper whisker is defined as either the maximum value or, if smaller, as the third quartile plus 1.5 times the interquartile range ($IQR = Q_3 - Q_1$); equally, the lower whisker is defined as the the minimum value or, if larger, as the first quartile minus the 1.5 times interquartile range. Continent panels are aligned ascendingly by the median of annual SSR trends from the left to the right, together with the world plot at the end. Four seasons (DJF, MAM, JJA, SON) and annual (ANN) trends are shown for each continent.

References

- Adedoyin, F., Ozturk, I., Abubakar, I., Kumeka, T., Folarin, O., and Bekun, F. V. (2020). Structural breaks in CO₂ emissions: Are they caused by climate change protests or other factors? *Journal of Environmental Management*, 266:110628.
- Arking, A. (1996). Absorption of solar energy in the atmosphere: Discrepancy between model and observations. *Science*, 273(5276):779–782.
- Bai, J. and Perron, P. (1998). Estimating and Testing Linear Models with Multiple Structural Changes. *Econometrica*, 66(1):47.
- Bai, J. and Perron, P. (2003). Computation and analysis of multiple structural change models. *Journal of Applied Econometrics*, 18(1):1–22.
- Boers, R., Brandsma, T., and Siebesma, A. P. (2017). Impact of aerosols and clouds on decadal trends in all-sky solar radiation over the Netherlands (1966–2015). *Atmospheric Chemistry and Physics*, 17(13):8081–8100.
- Breiman, L. (2001). Random forests. *Machine Learning*, 45:5–32.
- Budyko, M. I. (1969). The effect of solar radiation variations on the climate of the Earth. *Tellus*, 21(5):611–619.
- Cherian, R., Quaas, J., Salzmann, M., and Wild, M. (2014). Pollution trends over Europe constrain global aerosol forcing as simulated by climate models. *Geophysical Research Letters*, 41(6):2176–2181.
- CIESIN (2004). Global rural–urban mapping project (grump), alpha version: urban extents grids.
- Collins, F. C. (1995). *A comparison of spatial interpolation techniques in temperature estimation*. PhD thesis, Virginia Tech.
- Cró, S. and Martins, A. M. (2017). Structural breaks in international tourism demand: Are they caused by crises or disasters? *Tourism Management*, 63:3–9.
- Erxleben, J., Elder, K., and Davis, R. (2002). Comparison of spatial interpolation methods for estimating snow distribution in the Colorado Rocky Mountains. *Hydrological Processes*, 16(18):3627–3649.
- Firth, L., Hazelton, M. L., and Campbell, E. P. (2005). Predicting the onset of Australian winter rainfall by nonlinear classification. *Journal of Climate*, 18(6):772–781.
- Forkel, M., Carvalhais, N., Verbesselt, J., Mahecha, M., Neigh, C., and Reichstein, M. (2013). Trend Change Detection in NDVI Time Series: Effects of Inter-Annual Variability and Methodology. *Remote Sensing*, 5(5):2113–2144.
- Gilgen, H., Roesch, A., Wild, M., and Ohmura, A. (2009). Decadal changes in shortwave irradiance at the surface in the period from 1960 to 2000 estimated from Global Energy Balance Archive Data. *Journal of Geophysical Research*, 114(8):D00D08.
- Greenwald, R., Bergin, M. H., Xu, J., Cohan, D., Hoogenboom, G., and Chameides, W. L. (2006). The influence of aerosols on crop production: A study using the CERES crop model. *Agricultural Systems*, 89(2):390–413.
- Gupta, R., Somanathan, E., and Dey, S. (2017). Global warming and local air pollution have reduced wheat yields in India. *Climatic Change*, 140(3-4):593–604.

- Harris, I., Osborn, T. J., Jones, P., and Lister, D. (2020). Version 4 of the CRU TS monthly high-resolution gridded multivariate climate dataset. *Scientific Data*, 7(1).
- He, Y., Wang, K., Zhou, C., and Wild, M. (2018). A Revisit of Global Dimming and Brightening Based on the Sunshine Duration. *Geophysical Research Letters*, 45(9):4281–4289.
- Holben, B. N. (1986). Characteristics of maximum-value composite images from temporal AVHRR data. *International Journal of Remote Sensing*, 7(11):1417–1434.
- Jiang, Y. (2008). Prediction of monthly mean daily diffuse solar radiation using artificial neural networks and comparison with other empirical models. *Energy Policy*, 36(10):3833–3837.
- Leirvik, T. and Yuan, M. (2020). A machine learning technique for spatial interpolation of solar radiation observations. *Earth and Space Science Open Archive*, page 30.
- Moseid, K. O., Schulz, M., Storelvmo, T., Julsrud, I. R., Olivié, D., Nabat, P., Wild, M., Cole, J., and Takemura, T. (2020). Bias in CMIP6 models compared to observed regional dimming and brightening trends (1961–2014). *Atmospheric Chemistry and Physics*, pages 1–20.
- Müller, B., Wild, M., Driesse, A., and Behrens, K. (2014). Rethinking solar resource assessments in the context of global dimming and brightening. *Solar Energy*, 99:272–282.
- Myoung, B., Rhee, J., and Yoo, C. (2020). Long-Lead Predictions of Warm Season Droughts in South Korea Using North Atlantic SST. *Journal of Climate*, 33(11):4659–4677.
- Nabat, P., Somot, S., Mallet, M., Sanchez-Lorenzo, A., and Wild, M. (2014). Contribution of anthropogenic sulfate aerosols to the changing Euro-Mediterranean climate since 1980. *Geophysical Research Letters*, 41(15):5605–5611.
- NESDIS (1995). TerrainBase, Global 5 Arc-minute Ocean Depth and Land Elevation from the US National Geophysical Data Center (NGDC).
- Obryk, M. K., Fountain, A. G., Doran, P. T., Lyons, W. B., and Eastman, R. (2018). Drivers of solar radiation variability in the McMurdo Dry Valleys, Antarctica. *Scientific Reports*, 8(1):5002.
- Ohmura, A. and Gilgen, H. (1993). Re-Evaluation of the Global Energy Balance. pages 93–110. American Geophysical Union (AGU).
- Pfeifroth, U., Sanchez-Lorenzo, A., Manara, V., Trentmann, J., and Hollmann, R. (2018). Trends and Variability of Surface Solar Radiation in Europe Based On Surface- and Satellite-Based Data Records. *Journal of Geophysical Research: Atmospheres*, 123(3):1735–1754.
- Phillips, P. C., Leirvik, T., and Storelvmo, T. (2020). Econometric estimates of Earth’s transient climate sensitivity. *Journal of Econometrics*, 214(1):6–32.
- Proctor, J., Hsiang, S., Burney, J., Burke, M., and Schlenker, W. (2018). Estimating global agricultural effects of geoengineering using volcanic eruptions. *Nature*, 560(7719):480–483.
- Qin, W., Wang, L., Zhang, M., Niu, Z., Luo, M., Lin, A., and Hu, B. (2019). First effort at constructing a high-density photosynthetically active radiation dataset during 1961–2014 in China. *Journal of Climate*, 32(10):2761–2780.
- Roderick, M. L. and Farquhar, G. D. (2012). Geoengineering: Hazy, cool and well fed?
- Sanchez-Lorenzo, A., Calbó, J., and Wild, M. (2013). Global and diffuse solar radiation in Spain: Building a homogeneous dataset and assessing their trends. *Global and Planetary Change*, 100:343–352.

REFERENCES

- Sanchez-Lorenzo, A., Enriquez-Alonso, A., Wild, M., Trentmann, J., Vicente-Serrano, S. M., Sanchez-Romero, A., Posselt, R., and Hakuba, M. Z. (2017). Trends in downward surface solar radiation from satellites and ground observations over Europe during 1983–2010. *Remote Sensing of Environment*, 189:108–117.
- Sanchez-Lorenzo, A., Wild, M., Brunetti, M., Guijarro, J. A., Hakuba, M. Z., Calbó, J., Mystakidis, S., and Bartok, B. (2015). Reassessment and update of long-term trends in downward surface shortwave radiation over Europe (1939–2012). *Journal of Geophysical Research*, 120(18):9555–9569.
- Scudiero, E., Corwin, D. L., Morari, F., Anderson, R. G., and Skaggs, T. H. (2016). Spatial interpolation quality assessment for soil sensor transect datasets. *Computers and Electronics in Agriculture*, 123:74–79.
- Soares, P. M., Brito, M. C., and Careto, J. A. (2019). Persistence of the high solar potential in Africa in a changing climate. *Environmental Research Letters*, 14(12):124036.
- Storelvmo, T., Leirvik, T., Lohmann, U., Phillips, P. C. B., and Wild, M. (2016). Disentangling greenhouse warming and aerosol cooling to reveal Earth’s climate sensitivity. *Nature Geoscience*, 9:286–289.
- Sun, H., Gui, D., Yan, B., Liu, Y., Liao, W., Zhu, Y., Lu, C., and Zhao, N. (2016). Assessing the potential of random forest method for estimating solar radiation using air pollution index. *Energy Conversion and Management*, 119:121 – 129.
- Vu, T. T., Kiesel, J., Guse, B., and Fohrer, N. (2019). Analysis of the occurrence, robustness and characteristics of abrupt changes in streamflow time series under future climate change. *Climate Risk Management*, 26:100198.
- Wang, K., Ma, Q., Wang, X., and Wild, M. (2014). Urban impacts on mean and trend of surface incident solar radiation. *Geophysical Research Letters*, 41(13):4664–4668.
- Wild, M. (2009). Global dimming and brightening: A review. *Journal of Geophysical Research*, 114(D10):D00D16.
- Wild, M. (2012). Enlightening Global Dimming and Brightening. *Bulletin of the American Meteorological Society*, 93(1):27–37.
- Wild, M. (2016). Decadal changes in radiative fluxes at land and ocean surfaces and their relevance for global warming. *Wiley Interdisciplinary Reviews: Climate Change*, 7(1):91–107.
- Wild, M., Gilgen, H., Roesch, A., Ohmura, A., Long, C. N., Dutton, E. C., Forgan, B., Kallis, A., Russak, V., and Tsvetkov, A. (2005). From dimming to brightening: Decadal changes in solar radiation at earth’s surface. *Science*, 308(5723):847–850.
- Wild, M., Grieser, J., and Schär, C. (2008). Combined surface solar brightening and increasing greenhouse effect support recent intensification of the global land-based hydrological cycle. *Geophysical Research Letters*, 35(17).
- Wild, M. and Liepert, B. (2010). The Earth radiation balance as driver of the global hydrological cycle.
- Wild, M., Ohmura, A., Schär, C., Müller, G., Folini, D., Schwarz, M., Zytka Hakuba, M., and Sanchez-Lorenzo, A. (2017). The Global Energy Balance Archive (GEBA) version 2017: A database for worldwide measured surface energy fluxes. *Earth System Science Data*, 9(2):601–613.

- Wild, M., Wacker, S., Yang, S., and Sanchez-Lorenzo, A. (2021). Evidence for Clear-sky Dimming and Brightening in Central Europe. *Geophysical Research Letters*, page e2020GL092216.
- Xu, T., Guo, Z., Liu, S., He, X., Meng, Y., Xu, Z., Xia, Y., Xiao, J., Zhang, Y., Ma, Y., and Song, L. (2018). Evaluating Different Machine Learning Methods for Upscaling Evapotranspiration from Flux Towers to the Regional Scale. *Journal of Geophysical Research: Atmospheres*, 123(16):8674–8690.
- Yang, S., Wang, X. L., and Wild, M. (2018). Homogenization and trend analysis of the 1958-2016 in situ surface solar radiation records in China. *Journal of Climate*, 31(11):4529–4541.
- Zhou, Q., Flores, A., Glenn, N. F., Walters, R., and Han, B. (2017). A machine learning approach to estimation of downward solar radiation from satellite-derived data products: An application over a semi-arid ecosystem in the us. *PloS one*, 12(8):e0180239.

Appendices

APPENDIX A

Supporting Information for Paper 1

A.1 Dataset Description

Figure A.1 shows a map of the distribution of GEBA stations.

A.2 RF model Parameter Tuning

The tuning of the number of bootstraps is shown in Figure A.2. We choose the parameter value, 700, that the R^2 reach a high level and are relatively stable. Likewise, the number of candidate independent variables is set to 8 (Figure A.3).

A.3 Results

A.3.1 Model Evaluation

Figure A.4 shows a scatter plot of predicted values against observed values for each continent respectively. We see that the regression coefficients of the regression lines are reasonably close to 1 and the intercept terms are relatively small compared to the magnitude of average SSR levels. Although the models perform differently among the continents (e.g., better performance in North America and Europe, less ideal performance in South America and Africa), in general, the models are able to capture the variation of SSR. Caution needs to be taken when interpreting the high levels of R^2 . Because the R^2 are calculated based on raw values of SSR, they might have a systematic bias toward large values caused by the strong seasonality of monthly SSR.

A.3.2 Continental Average Trend Analysis

When calculating the global/continental average SSR of month t (\bar{R}_t), each grid ($R_{i,t}$) is weighted by the *cosine* of the latitude, which is given by:

$$\bar{R}_t = \sum_{i=1}^N w_i R_{i,t} \quad (\text{A.1})$$

where

$$w_i = \frac{\cos(\text{latitude}_i)}{\sum_i \cos(\text{latitude}_i)}, \text{latitude}_i \in \left[-\frac{\pi}{2}, \frac{\pi}{2}\right] \quad (\text{A.2})$$

The weighting procedure is to account for that the areas of grid boxes reduce with increasing latitude. By using the weight of *cosine* of latitude, it means to apply a weight of one for grid cells at the equator (which have 0 rad latitude, and therefore assigned a weight of $\cos(0) = 1$), and to apply a weight of zero for grid cells at the poles (which have $\frac{\pi}{2} \text{ rad}$ latitude, and a weight of $\cos(\frac{\pi}{2}) = 0$).

For the entire globe as well as each continent, monthly anomalies of global/continental average SSR are calculated and visualized in figures. Also shown are the regression lines for the entire period 1961-2019 and for the sub-segments separated by the detected breakpoints (refer to main paper Table 4 for the breakpoints as well as the slope coefficients).

[Figure A.5](#)—[Figure A.11](#) show the monthly anomaly figures in what follows.

World

Monthly anomalies [Figure A.5](#)

Europe

Monthly anomalies [Figure A.6](#)

Africa

Monthly anomalies [Figure A.7](#)

Asia

Monthly anomalies [Figure A.8](#)

Oceania

Monthly anomalies [Figure A.9](#)

North America

Monthly anomalies [Figure A.10](#)

South America

Monthly anomalies [Figure A.11](#)

List of Figures

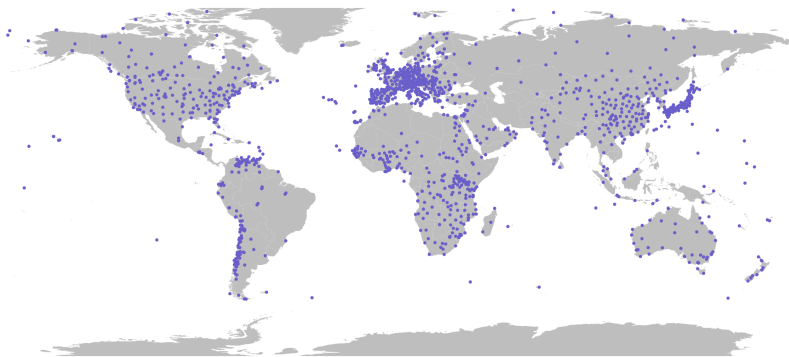


Fig. A.1 Station distribution in the GEBA dataset

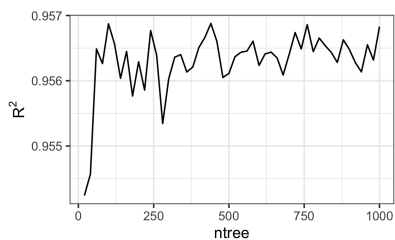


Fig. A.2 R^2 changing with the number of decision trees

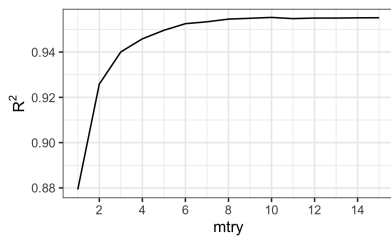


Fig. A.3 R^2 changing with the number of randomly preselected predictor variables

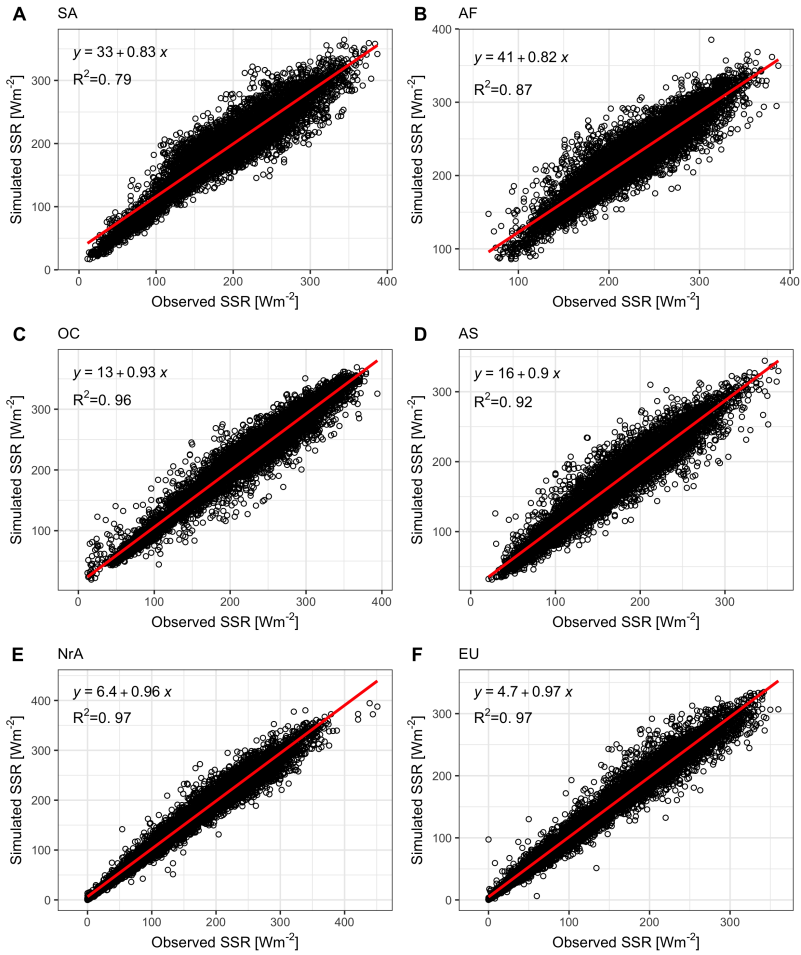


Fig. A.4 Simulation against observation raw values of SSR. The red line is obtained by regressing simulated SSR on observed SSR, also shown in each panel are the corresponding equation and R squared.

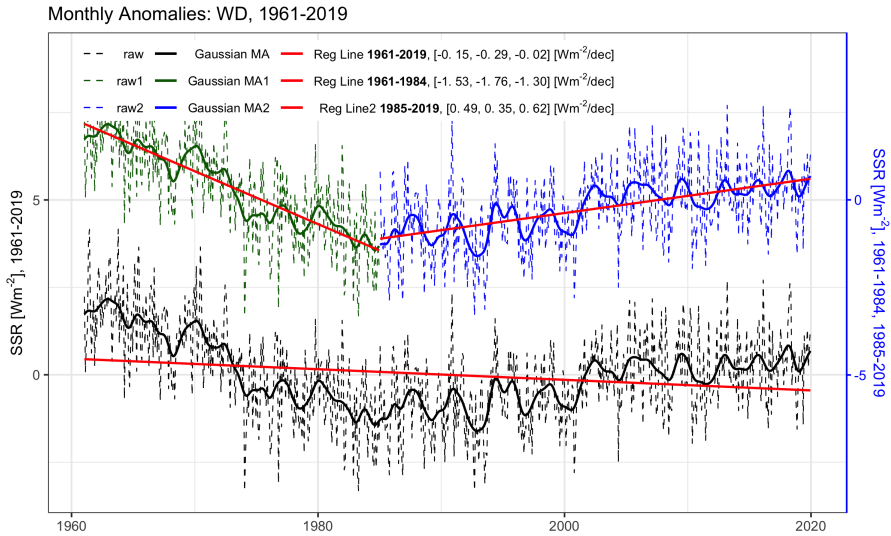


Fig. A.5 SSR global monthly anomalies over the time period 1961-2019 (left axis, lower black lines), and over segments divided by its breakpoint at 1984 (right axis, upper lines), namely, the first segment over 1961-1984 (dark green lines), and the second segment over 1985-2019 (blue lines). Raw monthly anomaly series are shown by the dashed lines, expressed as anomalies from the mean over the entire period. Additionally shown are the smoothed series by 12-month Gaussian filter (solid lines) and the linear decadal regression lines (red solid lines). The values in the brackets show the mean trend, lower 95% percentile, and upper 95% percentile, respectively. Note that the right axis is shifted by $+5 \text{ Wm}^{-2}$ from the left axis in order to separate the two series.

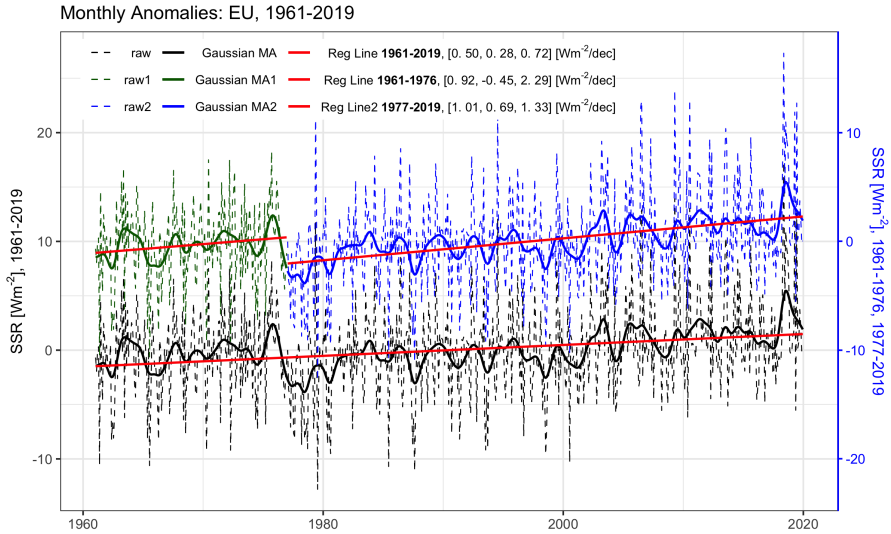


Fig. A.6 SSR monthly anomalies for Europe. Legends are the same as those of [Figure A.5](#), though two time segments here are 1961-1976 and 1977-2019.

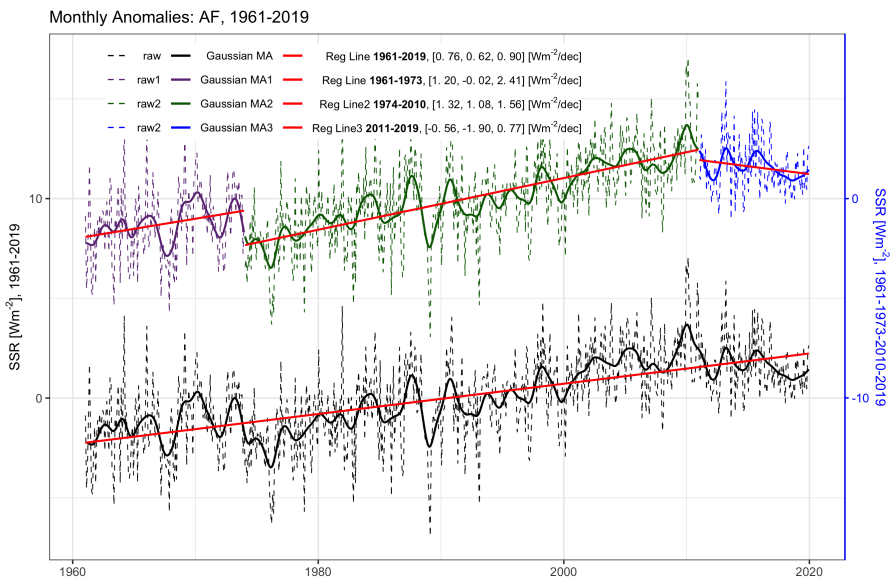


Fig. A.7 SSR monthly anomalies for Africa.

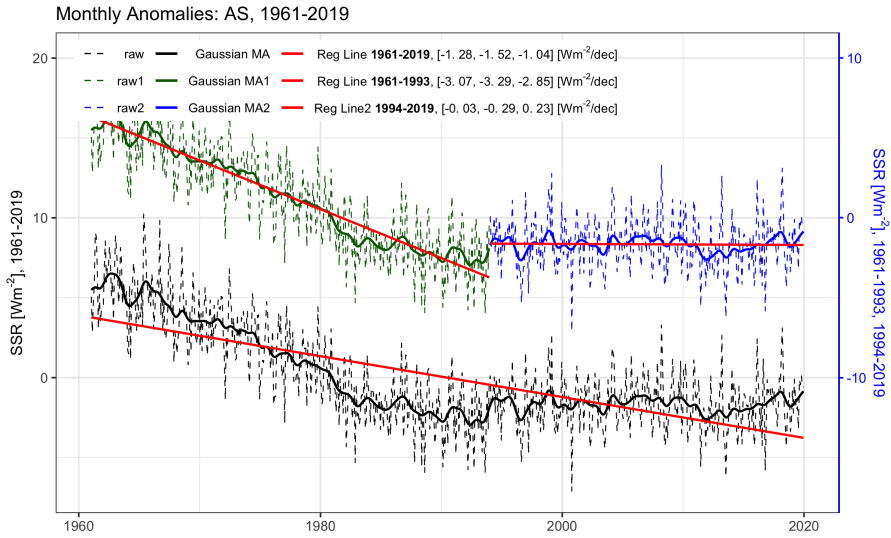


Fig. A.8 SSR monthly anomalies for Asia.

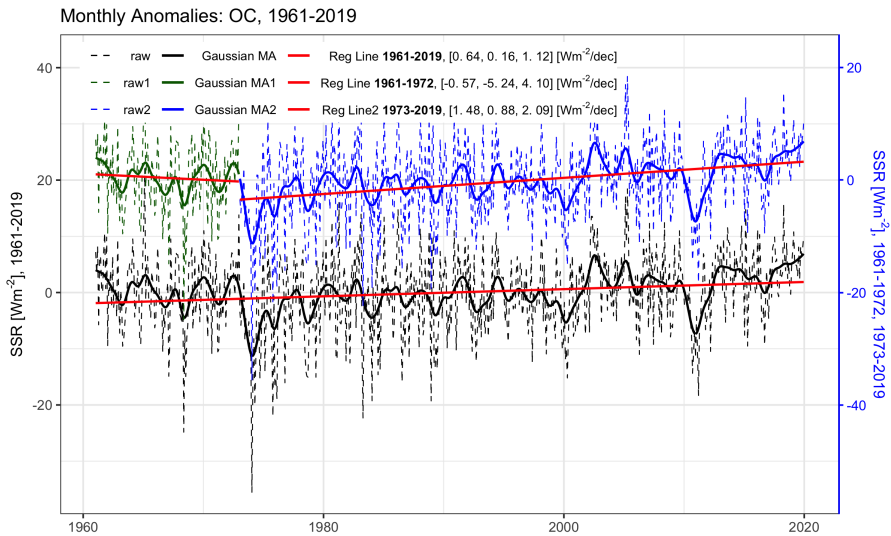


Fig. A.9 SSR monthly anomalies for Oceania.

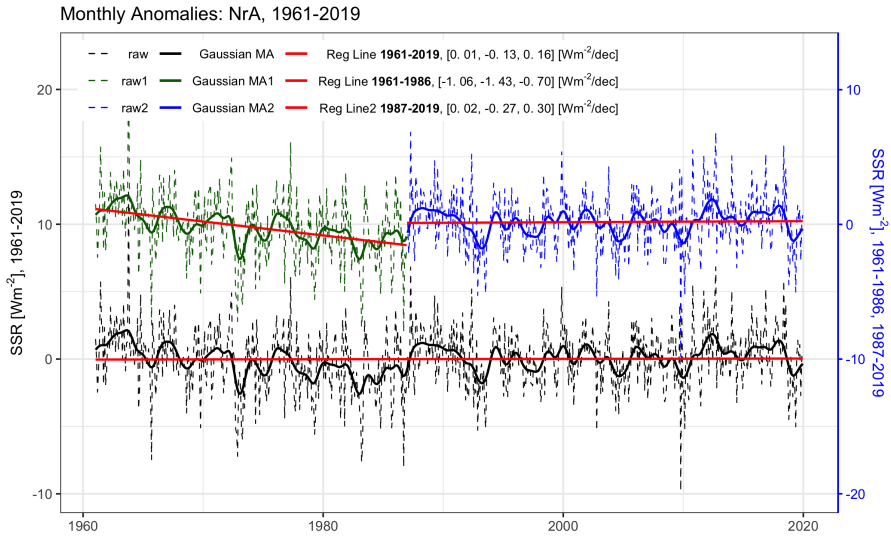


Fig. A.10 SSR monthly anomalies for North America.

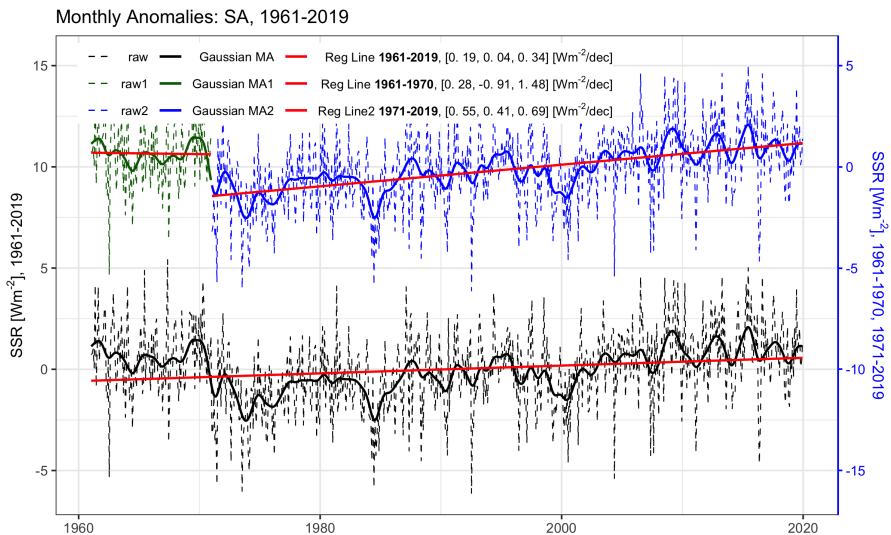


Fig. A.11 SSR monthly anomalies for South America.

Utgitt i ph.d. serie ved Handelshøgskolen:

- Nr. 1 – 2003 Lars Øystein Widding
Bygging av kunnskapsreservoarer i teknologibaserte nyetableringer
- Nr. 2 – 2005 Pawan Adhikari
Government Accounting in Nepal: Tracing the Past and the Present
- Nr. 3 – 2005 Tor Korneliussen
The Relationship between Initiation, Barriers, Product Quality and Internationalization
- Nr. 4 – 2005 Bjørn Willy Åmo
Employee innovation behavior
- Nr. 5 – 2005 Odd Birger Hansen
Regnskap og entreprenørskap. En fortolkende studie av hvordan to entreprenører bruker regnskap
- Nr. 6 – 2006 Espen John Isaksen
Early Business Performance
- Initial factors effecting new business outcomes
- Nr. 7 – 2006 Konstantin Timoshenko
Russian Government Accounting:
Changes at the Central level and at a University
- Nr. 8 – 2006 Einar Rasmussen
Facilitating university spin-off ventures
-an entrepreneurship process perspective
- Nr. 9 – 2007 Gry Agnete Alsos
Portfolio Entrepreneurship - general and farm contexts
- Nr. 10 – 2007 Elsa Solstad
Tre sykehus - to verdener - en fusjon.
En studie av reorganisering i et helseforetak
- Nr. 11 – 2007 Levi Gårseth-Nesbakk
Experimentation with accrual accounting at the central government level in Norway - how a global phenomenon becomes a local practice
- Nr. 12 – 2007 Tatiana Iakovleva
Factors Associated with new venture performance:
The context of St. Petersburg

- Nr. 13 – 2007 Einar Lier Madsen
Utvikling av dynamiske kapabiliteter i små og mellomstore bedrifter
- Nr. 14 – 2008 Anne Haugen Gausdal
'Network Reflection' – a road to regional learning, trust and innovation
- Nr. 15 – 2008 Lars Rønning
Social capital in farm-based entrepreneurship and rural development
- Nr. 16 – 2008 Terje Andreas Mathisen
Public Passenger Transport in Norway – Regulation, Operators' Cost Structure and Passengers' Travel Costs
- Nr. 17 – 2008 Evgueni Vinogradov
Immigrant Entrepreneurship in Norway
- Nr. 18 – 2008 Elin Oftedal
Legitimacy of Creative Destruction
- Nr. 19 – 2009 Frode Kjærland
Valuation of Generation Assets – a Real Option Approach
- Nr. 20 – 2009 Tatiana Maximova-Mentzoni
Marketization of the Russian University: Origins, Features and Outcomes
- Nr. 21– 2009 Hugo Skålsvik
Studies of Market led Processes influencing Service Performance:
-Case Studies on the Norwegian Coastal Voyage
- Nr. 22– 2009 Svein Oskar Lauvsnes
Determinants of a shifting effective demand equilibrium.
An explorative investigation of the interaction between
psychological, financial and real factors
- Nr. 23– 2010 Frode Fjelldal-Soelberg
Entreprenøriell markedsføring. En studie av entreprenørskap og markeds-
føring som overlappende fenomen
- Nr. 24– 2010 Heidi Rapp Nilsen
From Weak to Strong Sustainable Development
An analysis of Norwegian economic policy tools in mitigating climate
change

- Nr. 25– 2010 Gowindage Chamara Jayanath Kuruppu
Development of Central Government Accounting in Sri Lanka:
Three perspectives on the accounting changes
- Nr. 26– 2010 Marina Z. Solesvik
Interfirm collaboration: The context of shipbuilding.
- Nr. 27– 2010 Jan Terje Henriksen
Planning, Action and Outcome
- Evaluation of the Norwegian Petroleum System:
A Structuration Approach to Ripple Effect Studies
- Nr. 28– 2010 May Kristin Vespestad
Empowered by Natures – Nature-based High North Tourism Experiences
in an International Context
- Nr. 29– 2011 Andrei Mineev
How has the petroleum supply industry developed in The Russian Barents
Sea Region? Institutional and managerial aspects
- Nr. 30– 2011 Jorunn Grande
Entrepreneurship in small rural firms - the case of agriculture
- Nr. 31– 2011 Thomas Johansen
Paradigms in Environmental Management Research:
Outline of an Ecosophical-Hermeneutic Alternative
- Nr. 32– 2011 Elena Dybtsyna
Accountant in Russia: changing times, changing roles.
- Nr. 33– 2012 Harald Fardal
Information Systems Strategy in Practice
A Social Process Perspective
- Nr. 34– 2012 Kristin Haugland Smith
Hva er bedrifters samfunnsansvar?
- En empirisk tilnærming av bedrifters ansvar overfor samfunnet
- Nr. 35– 2012 Are Branstad
The management of entrepreneurship support
– Organisation and learning in corporate incubation, technology transfer
and venture capital
- Nr. 36– 2012 Victoria Konovalenko
A “coordination kaleidoscope”:
The role of a “Corporate University” as a coordinator of knowledge flows
in a Russian transnational corporation

- Nr. 37– 2012 Thor-Erik Sandberg Hanssen
Essays in Transport Economics with application to Transport Policy
- Nr. 38– 2013 Are Severin Ingulfsvann
Verdiforskynning i friluftslivet i lys av økologisk økonomi
- Nr. 39– 2013 Natalia Andreassen
Sustainability Reporting in a Large Russian Oil Corporation.
Production Safety Issues
- Nr. 40– 2013 Elena Panteleeva
Contemporary Management Accounting Practices in Russia:
The Case of a Subsidiary in a Russian Oil Company
- Nr. 41– 2013 Thusitha S.L.W.Gunawardana
Impact of Power Sources on Channel Members' Performance
- Nr. 42– 2013 Nadezda Nazarova
Mastering Nature and Managing Frictions: Institutional Work and Supply
Chain Management in the High North
- Nr. 43– 2013 Inge Hermanrud
Managed Networks of Competence in Distributed Organizations
- The role of ICT and Identity Construction in Knowledge Sharing
- Nr. 44– 2013 Kari Djupdal
Sustainable entrepreneurship:
outcomes associated with an environmental certification resource
- Nr. 45– 2013 Imtiaz Badshah
Federal government accounting in The Islamic Republic of Pakistan
- Nr. 46– 2014 Muhammad Arif
Inter-organizational Exchange Relationships
– Exchange Relationships between Local Service Suppliers and Tour
Operators in the Tourism Distribution Channel
- Nr. 47– 2014 Wondwesen Tafesse
The Marketing Functions of the Trade Show System
- Nr. 48– 2014 Fritz J. Nilssen
Erfaringsutveksling som grunnlag for mestring og livskvalitet
Diagnoseoverskridende samtalegrupper for familier med barn som har
nedsatt funksjonsevne og eller kronisk sykdom.

- Nr. 49– 2014 Ingebjørg Vestrum
The Resource Mobilisation Process of Community Ventures
-The Case of Cultural Events in Rural Communities
- Nr. 50– 2014 Ragnhild Johnson
The Practice of Project Management
- A qualitative analysis of complex project-based organizations
- Nr. 51– 2014 Ann Heidi Hansen
Memorable moments
Consumer immersion in nature-based tourist experiences
- Nr. 52– 2014 June Borge Doornich
Entry modes and organizational learning during internationalization
An analysis of Norwegian supply companies' entering and expanding in
the Russian oil and gas sector
- Nr. 53– 2014 Kjersti Karijord Smørvik
Opplevelsesskaping i dynamiske opplevelsesrom:
En studie av turistenes opplevelser på Hurtigruten
- Nr. 54– 2015 Marianne Terese Steinmo
How Firms use University-Industry Collaboration to Innovate:
The role and Development of Social Capital and Proximity Dimensions
- Nr. 55– 2015 Eva J.B. Jørgensen
Border Firms: Norway and Russia
- Nr. 56– 2015 Krister Salamonsen
Exogenous Shocks as Drivers of Growth in Peripheral Regions.
- A Multilevel Approach to Regional Development
- Nr. 57– 2015 Hindertje Hoarau Heemstra
Practicing open innovation in experience-based tourism:
the roles of knowledge, values and reflexivity
- Nr. 58– 2015 Elena Zhurova
Environmental Performance Reporting of Russian Oil and Gas Companies
- Nr. 59– 2016 Siri Jakobsen
Environmental innovation cooperation:
The development of cooperative relationships between Norwegian firms
- Nr. 60– 2016 Antonina Tsvetkova
Supply Chain Management in the Russian Arctic:
An institutional perspective

- Nr. 61– 2017 Kjersti Granås Bardal
Impact of Adverse Weather on Road Transport:
Implications for Cost-Benefit Analysis
- Nr. 62– 2017 Kristian Støre
Methodological contributions and applications in real options analysis
- Nr. 63– 2017 Thomas André Lauvås
The dynamics of university-industry collaboration:
A longitudinal case study of research centers
- Nr. 64– 2017 Sølvi Solvoll
Development of effectual and casual behaviors:
Exploring new venture creation in the tourism industry
- Nr. 65– 2017 Evgenii Aleksandrov
The changing role of accounting from reformees' perspective:
A study of public sector reforms in Russia
- Nr. 66– 2017 Igor Khodachek
Budget, Strategy and Accounting.
Managing institutional change in Russia's governments
- Nr. 67– 2018 Vivi Marie Lademo Storsletten
Quality as flourishing
A study of quality based upon leadership in kindergartens with
implications for Ecological Economics
- Nr. 68– 2018 Olga Iermolenko
The human side of accounting:
The bonds between human agency and management accounting
practices' changes in the transitional economy
- Nr. 69– 2018 Karin Wigger
Mobilization of Collective Resources for Entrepreneurship:
Case Studies in Nordic Peripheries
- Nr. 70 – 2018 Andreas Mikkelsen
Trading fast and slow: algorithmic trading in the Nordic region
- Nr. 71 – 2018 Asbjørn Veidal
Strategic entrepreneurship in farm businesses
- Nr. 72 – 2018 Are Jensen
Early imprints in and on new technology-based firms

- Nr. 73 – 2018 Marianne Arntzen-Nordqvist
The financing process of new technology-based firms
- The entrepreneur's perspective
- Nr. 74 – 2019 Irina Nikolskaja Roddvik
Deprivation of control: A driving force to gain influence during
the internationalization process of MNC
- Nr. 75 – 2019 Petter Gullmark
Unraveling the Building Blocks of Local Government Organizations'
Innovativeness: Insights from a Dynamic Capabilities Perspective
- Nr. 76 – 2019 Hanne Stokvik
Knowledge for Innovation
- Nr. 77 – 2019 Anastasiya Henk
Between the Devil and the Deep Blue Sea: Managing Business Processes
in Turbulent Environments
- Nr. 78 – 2019 Tadeu Fernando Nogueira
Entrepreneurial Learning: An Exploration of the Learning of
New Venture Founders
- Nr. 79 – 2020 Veronika Vakulenko
Public Sector Reforms in Ukraine: Roles Played by Global and Local
Agents in Implementing Converging and Diverging Changes
- Nr. 80 – 2020 Lars Hovdan Molden
Adapting to Change - On the Mechanisms of Dynamic Capabilities
- Nr. 81 – 2020 Sudip Kranti Tiwari
Navigating International Entrepreneurship in a Developing Economy Con-
text: Lessons from Nepal
- Nr. 82 – 2020 Vu Le Tran
Expected Returns: An Empirical Asset Pricing Study
- Nr. 83 – 2020 Marit Breivik-Meyer
It takes two to tango:
The role of incubators in the early development of start-ups
- Nr. 84 – 2021 Per Ivar Seljeseth
Assessing Outcomes from Business-to-Business Selling
- Nr. 85 – 2021 Amsale Kassahun Temesgen
Human Wellbeing and Local-level Sustainability

- Nr. 86 – 2021 Ensieh Roud
The Role of Joint Training in Inter-organizational Collaboration in Emergency Management
- Nr. 87 – 2021 Menghan Yuan
Climate Change and Economic Growth: An Empirical Study of Economic Impacts of Climate Change

Global warming and the increasing incidence of extreme weather events are disrupting economies and affecting human lives over the world. This thesis intends to constrain the uncertainty of climate sensitivity and to investigate the economic impacts of climate change. This thesis consists of four papers.

The first two papers aim to address the uncertainty of the climate sensitivity. The authors applied an empirical estimation framework which relates temperature to solar radiation and CO_2 in a cointegrating equilibrium relationship. In order to facilitate the empirical estimation, the first paper constructs a global dataset of surface solar radiation with complete global land surface coverage during the period 1961-2019, which provides the input data for the climate sensitivity estimation conducted in the second paper. The second paper empirically estimates Transient Climate Sensitivity (TCS) for 22 global climate models and significantly narrows the confidence interval of TCS compared to previous estimates.

The last two papers use panel data analyses to examine how agriculture and aggregated economies are influenced by climate change, respectively. Based on an extensive dataset covering worldwide countries over more than five decades, the agricultural paper contributes to investigate the heterogeneity effects in various regions and in rich/poor countries. The last paper investigates the possibility of using a novel panel data approach—interactive fixed effects model, to allow for the heterogeneous effects of countries affected by the common global shocks.